Microscopic Assessment of Corrosion-Induced Cracking in Reinforced Concrete Using the Damage Rating Index

GOLSHID NOORI DOLOOEE

Thesis submitted to the University of Ottawa
in partial fulfillment of the requirements for the degree of

MASTER OF APPLIED SCIENCE IN CIVIL ENGINEERING

Under the supervision of Dr. Beatriz Martín-Pérez and Dr. Leandro Sanchez

Department of Civil Engineering
Faculty of Engineering
University of Ottawa

Abstract

Corrosion of embedded reinforcement remains one of the most critical deterioration mechanisms compromising the longevity and serviceability of reinforced concrete (RC) structures. The Damage Rating Index (DRI), a microscopic technique that has been employed for assessing concrete damage induced by internal swelling reactions, has not yet been applied to the assessment of reinforcement corrosion-induced damage. This study investigates the applicability and sensitivity of the DRI protocol in evaluating corrosion-induced cracking in the RC. A series of cylindrical RC specimens with two water-to-cement ratios (0.4 and 0.54) and a range of concrete cover-to-rebar diameter ratios were subjected to accelerated corrosion to achieve a target reinforcing steel mass loss of 5% embedded.

Microscopic examination and DRI quantification were conducted on polished sections of concrete, focusing on two key deterioration features: cracks in the cement paste (CCP) and cracks with reaction products in the cement paste (CCP-RP). The findings demonstrate that the DRI effectively captures variations in damage pattern and severity as a function of mixture design and cover depth. An extended DRI approach, incorporating normalized crack densities and area-based analyses, further substantiated the sensitivity of the method. A corrosion damage classification model was proposed, integrating DRI counts, normalized crack areas, and visual observations to define five progressive levels of deterioration. The results establish the DRI as a viable diagnostic tool for quantifying microstructural damage due to reinforcement corrosion, marking the first demonstration of its application beyond internal swelling reactions and underscoring its potential as a broader framework for structural durability assessment.

Keywords: Damage Rating Index (DRI); corrosion-induced cracking; reinforced concrete; cement paste cracking; durability assessment

Acknowledgements

This thesis represents the culmination of a journey made possible by the unwavering support and guidance of many individuals. I extend my deepest gratitude to my supervisors, Dr. Beatriz Martín-Pérez and Dr. Leandro Sanchez. Their combined expertise, thoughtful mentorship, and continuous encouragement were instrumental throughout all stages of this research. Their critical feedback and insightful discussions helped refine the methodology and enhance the overall quality and scientific depth of this work. I am sincerely thankful for the opportunity to learn from both.

I would also like to thank the Technical Officers (TOs) of the structural laboratory for their essential contributions to the experimental phase of this research. Their technical expertise and commitment to quality ensured the accuracy and success of the laboratory work.

My sincere appreciation extends to Rennan Medeiros for his invaluable assistance and consistent support throughout this research. Your input and encouragement played a crucial role in the completion of this work.

To my friends and family, thank you for your enduring support, encouragement, and belief in me during every stage of this journey.

Lastly, to my best friend and love, Soroush—your presence and encouragement have been a source of strength throughout this endeavor. This achievement is as much yours as it is mine.

Table of Contents

List of Tables viii

List of Figures ix

1 Introduction 1

1.1 Background 1

1.2 Research Objectives 2

1.3 Organization of Thesis 3

1.4 References 4

2 Literature Review 6

2.1 Corrosion in Reinforced Concrete 7

2.1.1 Corrosion Initiation 8

2.1.2 Corrosion Propagation 8

2.1.3 Corrosion in Concrete: Causes and Mechanisms 10

2.1.3.1 Carbonation-induced corrosion 11

2.1.3.2 Chloride-induced corrosion 12

2.1.1 Corrosion-Induced Damage in the RC 14

2.2 Assessment Tools for Corrosion-Induced Cracking in RC 15

2.1.4 Manual and Visual Assessment of Cracking 15

2.1.5 Infrared Thermography (IRT) 16

2.1.6 Digital Image Correlation (DIC) 17

2.1.7 Ultrasonic Pulse Velocity (UPV) 18

2.1.8 Impact Echo (IE) 18

2.1.9 Acoustic Emission (AE) 19

2.1.10 Ground Penetration Radar (GPR) 20
2.1.11 X-ray Computed Tomography (CT) 20
2.1.12 Petrographic Analysis as a Basis for Quantifying Concrete Durability 21
2.3 Damage Rating Index (DRI) 23
2.3.1 DRI Protocol 25
2.3.1.1 Samples Preparation for DRI 26
2.3.1.2 Classification of Features of Deterioration 27
2.3.1.2.1. Closed or line cracks in aggregate particles 29
2.3.1.2.2. Open crack in the aggregate 29
2.3.1.2.3. Open crack in the aggregate with reaction products 30
2.3.1.2.4. Cracks in cement paste 31
2.3.1.2.5. De-bonded aggregate 31
2.3.1.2.6. Disaggregated particle 32
2.3.1.3 Extended Version of the DRI 32
2.4 Critical Evaluation of DRI Methodology through Literature Analysis 33
2.5 Research Gap 37
2.6. References 38
3 Research Methodology 46
3.1 Overview 46
3.2 Test Specimens 46
3.3 Materials and Mixture Proportions 48
3.4 Casting and Curing 50
3.5 Compressive Strength 51

3.6 Accelerated Corrosion Regime 52
3.7 Damage Rating Index: The Method 56
3.7.1 Samples Preparation and Polishing 56
3.8 References 58
4 Assessment of the Damage Rating Index (DRI) as a Tool for Quantifying Corrosion-Induced Damage in Reinforced Concrete 59
4.1 Introduction 59
4.1.1 Corrosion-Induced Cracking 60
4.1.2 The Damage Rating Index (DRI) 61
4.2 Research Significance 64
4.3 Materials and Methods 65
4.3.1 Materials and Mixture Proportions 65
4.3.2. Curing and Accelerated Corrosion of Test Specimens 67
4.3.2 Methods for Assessment and Analysis 68
4.3.3 DRI-Based Analysis 69
4.4 Results 70
4.4.1 Quantitative Assessment of Damage Using DRI 70
4.4.2 Impact of W/C and C/D on Corrosion-Induced Deterioration 72
4.5 Discussion 73
4.5.1 Sensitivity of the DRI to Evaluating Corrosion-Induced Damage 73
4.5.2 Damage Classification Framework 74
4.6. Conclusions 81
4.7. References 83
5 Concluding Remarks 87

5.1. Conclusions 87

5.2. Recommendations for Future Work 88

List of Tables

Table 2-1 - DRI weighing factors first implemented, Adapted from Clemeña et al. (2000); P.E. Grattan-Bellew; A. Danay (1992); Shrimer (2006); Sims (1992) 24

Table 2-2 - Types of deterioration features and current weighting factors of the DRI 27

Table 3-1 - Details of test specimens with geometries, reinforcement, and corrosion parameters 48

Table 3-2 - Material type, mix-design proportions and properties 49

Table 4-1 - (a) DRI distress features and weighting factors, adopted from Villeneuve et al. (2012) 63

Table 4-2 - Cylinder geometries and C/D ratios 66

Table 4-3 - Characteristics of materials 66

Table 4-4 - Concrete mix proportions 67

Table 4-5 - Compressive strength test results for concrete cylinders 67

Table 4-6 - DRI assessment results of corrosion - affected concrete 79

List of Figures

Figure 2-1 - The steel corrosion process, adapted from Broomfield (2007) 10

Figure 2-2 - Volume relationships between iron and its oxides according to the corrosion process adapted, from Broomfield (2007) 10

Figure 2-3 - The mechanism of carbonation-induced corrosion in RC, adapted from Rodrigues et al. (2021) 12

Figure 2-4 - The mechanism of chloride-induced corrosion, adapted from Rodrigues et al. (2021) 13

Figure 2-5 - Chloride-induced corrosion: exploring varied outcomes in high and low chloride environments, adapted from Rodrigues et al. (2021) 13

Figure 2-6 - (a) DRI sample cutting (b) sample before grinding (c) handheld polisher 26

Figure 2-7 - (a) A well-polished, highly reflective surface featuring a grid, with visible light reflection in the bottom-right corner (b) a 3D-printed grid positioned over the polished surface, adapted from Sanchez, (2024) 27

Figure 2-8 - Closed cracks in the aggregate particles 29

Figure 2-9 - Open cracks in the aggregate particles 30

Figure 2-10 - Open cracks in the aggregate particles with reaction products 30

Figure 2-11 - Cracks in the cement paste without reaction products 31

Figure 2-12 - Cracks in the cement paste with reaction products 31

Figure 2-13 - Debonded aggregate particles 32

Figure 2-14 - AAR damage model links 0.05–0.30% expansion to Type A (sharp) and Type B (onionskin) cracks adapted, from Sanchez et al. (2016) 34

Figure 2-15 - DRI charts, adapted from Sanchez et al. (2016) 35

Figure 2-16 - Crack density as a function of expansion, adapted from Sanchez et al. (2015) 37

Figure 3-1- Concrete cylinder dimensions 47

Figure 3-2 - Concrete cylinders with centrally reinforcing steel bars prior to casting & (b) Concrete cylinders immediately after casting 50

Figure 3-3 - Concrete specimens after 28 days of curing, ready for accelerated corrosion test ... 51

Figure 3-4 - Concrete specimens during compressive strength test 51

Figure 3-5 - Compressive strength test results for concrete cylinders 52

Figure 3-6 - (a)Natural burlap fabric used for moisture retention in accelerated corrosion regime (b) Stainless steel wire mesh used as cathode in the accelerated corrosion setup (c) Burlap-wrapped reinforced concrete cylinders with stainless steel mesh for corrosion testing 53

Figure 3-7 - Schematic of the impressed current setup, adapted from Bhattacharjee (2020)..... 55

Figure 3-8 - (a) Clamp connections to 10M and 20M rebar protrusions for accelerated corrosion (b) Specimen connected to power source; (c) Close-up of corroded rebar connection 55

Figure 3-9 - Accelerated corrosion setup: concrete specimens in NaCl solution connected to the power supply 56

Figure 3-10 - (a) unpolished & (b) polished concrete surface 57

Figure 3-11 - (a) One cm^2 mesh grid on the polished sample (b) microscopic analysis using the DRI protocol 57

Figure 4-1- (b) Features of deterioration of DRI in a 1 cm2 grid (Sanchez et al., 2018) 63

Figure 4-2 - (a) Reinforced concrete cylinder; (b) Parallel circuit 68

Figure 4-3 - DRI assessment for the different concrete specimens in the study..... 71

Figure 4-4 - Normalized crack densities of CCP and CCP-RP as a function of C/D ratios 73

Figure 4-5 - Percentage distribution of CCP and CCP-RP relative to total distress features (CCP + CCP-RP) for each mixture and C/D ratio 74

Figure 4-6- Visual Inspection of Crack Propagation 80

1 Introduction

1.1 Background

Reinforced concrete (RC) is a versatile and cost-effective construction material, recognized for its mechanical properties and enduring durability throughout its operational lifespan. However, its durability can be compromised by exposure to aggressive environments, with corrosion of steel reinforcement being one of the most critical challenges (Bertolini 2013; Mehta and Monteiro 2001). This results in corrosion by-products swelling between two to six times compared to the original volume, leading eventually to cracking, spalling, and delamination of the surrounding concrete, and ultimately deteriorating the concrete-reinforcement interface (Bertolini 2013; Hwang et al., 2023). Consequently, these defects compromise the bond between steel and concrete, reducing the structural performance and longevity of the RC structures (Tian et al., 2023).

Recent advancements in damage assessment tools, including non-destructive techniques (e.g., ground-penetrating radar, ultrasonic pulse velocity, and acoustic emission), and visual inspection methods, have provided valuable insights into the extent of cracking (Barbosh et al., 2022; Robles et al., 2022). However, these techniques often lack precision in characterizing internal conditions or are limited to advanced stages of deterioration. This highlights the need for a reliable protocol capable of accurately quantifying the extent of concrete deterioration induced by corrosion.

The Damage Rating Index (DRI), a microscopic and semi-quantitative petrographic tool, is a method increasingly recognized for its ability to assess the extent of damage in concrete affected by various deterioration mechanisms (Sanchez et al., 2015, 2017). While its effectiveness in quantifying damage caused by internal swelling reactions is well-established, its application to corrosion-induced cracking of concrete remains unexplored.

Therefore, this study focuses on investigating the applicability of DRI in assessing corrosion-induced cracking. An experimental laboratory campaign was carried out, in which concrete cylinders produced with varying diameters, water-to-cement ratios, steel rebar diameters, and cover depths were subjected to an accelerated corrosion regime for a target steel mass loss of 5% and the last version of DRI (Sanchez et al., 2015) was used to assess the extent and severity of the ensuing concrete damage.

1.2 Research Objectives

As previously discussed, the DRI has been widely used to assess damage from internal swelling reactions (ISR), but its applicability to corrosion-induced deterioration of concrete remains unexplored. This study aims to evaluate the applicability of the current DRI protocol in assessing corrosion-induced cracking, focusing on understanding its effectiveness as a diagnostic test protocol.

The objectives of this study are:

- **Assess the reliability and sensitivity of the DRI in evaluating corrosion-induced damage.**

This study investigates whether the DRI can effectively quantify the severity of corrosion-induced damage in reinforced concrete. By analyzing its reproducibility across different concrete conditions, mainly varying water-to-cement (W/C) and concrete cover-to-rebar diameter (C/D) ratios, the study evaluates its ability to distinguish between different patterns and extent of deterioration.

- **Develop a corrosion damage classification framework integrating DRI and visual observations.**

A qualitative corrosion-induced damage classification system is introduced by correlating DRI values, normalized crack area, and visual inspection data.

This study represents the first systematic application of the Damage Rating Index (DRI) to corrosion-induced deterioration in reinforced concrete, expanding its use beyond internal swelling reactions. The innovation lies in (i) demonstrating the DRI's sensitivity to corrosion-related microstructural features, (ii) introducing an extended DRI approach with normalized crack densities and areas, and (iii) developing a new corrosion damage classification framework that integrates microscopic (DRI) and macroscopic (visual inspection) indicators.

1.3 Organization of Thesis

This thesis is structured into five chapters, as detailed below:

Chapter 1 introduces the motivation for the study and the rational for applying the DRI protocol in corrosion-induced concrete cracking.

Chapter 2 reviews the mechanisms and impacts of corrosion on the RC structures, including initiation and propagation processes, and evaluates existing diagnostic tools for assessing damage caused by corrosion. Special focus is placed on the evolution and application of the DRI protocol, emphasizing its development as a semi-quantitative petrographic tool designed to systematically quantify damage in concrete resulting from deterioration mechanisms.

Chapter 3 provides an overview of the experimental research and methodology used to assess corrosion-induced cracking in the RC through the current version of the DRI protocol. This chapter outlines the testing matrix, sample features, and experimental setups utilized in the study. It covers the preparation of concrete samples, including material selection and reinforcement configurations, as well as the accelerated corrosion regime applied. Additionally, the chapter explains the DRI application to quantify petrographic features impacted by corrosion.

Chapter 4 is presented as a paper evaluating the applicability of the current version of the DRI as a diagnostic tool for quantifying corrosion-induced damage in the RC. The chapter outlines the experimental framework, including the preparation of specimens with varying W/C and C/D ratios, which were subjected to an accelerated corrosion regime. The findings demonstrate the potential of the DRI protocol in offering valuable insights into corrosion-induced deterioration and its variability across different specimen materials and detailing configurations. This work evaluates the applicability of the DRI for quantifying corrosion-induced deterioration in the RC. The results demonstrate that DRI effectively captures microstructural damage, particularly the development of cracks in the cement paste and cracks with reaction products in the cement paste, which serve as key indicators of corrosion severity. A classification of corrosion-induced damage levels based on the DRI is proposed, reinforcing its potential as a diagnostic tool for assessing reinforced concrete deterioration.

Finally, Chapter 5 concludes the thesis by summarizing key findings, discussing the implications of using the current version of the DRI for corrosion damage assessment, and proposing recommendations for future research to refine and expand its application.

1.4 References

Barbosh, M., K. Dunphy, and A. Sadhu. 2022. "Acoustic emission-based damage localization using wavelet-assisted deep learning." *Journal of Infrastructure Preservation and Resilience*, 3 (1). Springer Nature. https://doi.org/10.1186/s43065-022-00051-8.

Bertolini, Luca. 2013. *Corrosion of steel in concrete prevention, diagnosis, repair*. (Luca. Bertolini, ed.). Weinheim: Wiley-VCH.

Hwang, W., and K. Yong Ann. 2023. "Determination of rust formation to cracking at the steel–concrete interface by corrosion of steel in concrete." *Construction and Building Materials*, 367. Elsevier Ltd. https://doi.org/10.1016/j.conbuildmat.2022.130215.

Mehta, P. K., and P. J. M. Monteiro. n.d. "Concrete: Microstructure, Properties, and Materials."

Robles, K. P. V., J. J. Yee, and S. H. Kee. 2022. "Electrical Resistivity Measurements for Nondestructive Evaluation of Chloride-Induced Deterioration of Reinforced Concrete—A Review." *Materials*, 15 (8). MDPI. https://doi.org/10.3390/ma15082725.

Sanchez, L., T. Drimalas, B. Fournier, D. Mitchell, and J. Bastien. 2018. "Comprehensive damage assessment in concrete affected by different internal swelling reaction (ISR) mechanisms." *Cement and Concrete Research*, 107: 284–303. Elsevier Ltd. https://doi.org/10.1016/j.cemconres.2018.02.017.

Sanchez, L. F. M., B. Fournier, M. Jolin, M. A. B. Bedoya, J. Bastien, and J. Duchesne. 2016. "Use of Damage Rating Index to quantify alkali-silica reaction damage in concrete: Fine versus coarse aggregate." *ACI Materials Journal*, 113 (4): 395–407. American Concrete Institute. https://doi.org/10.14359/51688983.

Sanchez, L., B. Fournier, M. Jolin, D. Mitchell, and J. Bastien. 2017. "Overall assessment of Alkali-Aggregate Reaction (AAR) in concretes presenting different strengths and incorporating a

wide range of reactive aggregate types and natures." *Cement and Concrete Research*, 93: 17–31. Pergamon. https://doi.org/10.1016/J.CEMCONRES.2016.12.001.

Tian, Y., G. Zhang, H. Ye, Q. Zeng, Z. Zhang, Z. Tian, X. Jin, N. Jin, Z. Chen, and J. Wang. 2023. "Corrosion of steel rebar in concrete induced by chloride ions under natural environments." *Construction and Building Materials*, 369: 130504–130504. Elsevier. https://doi.org/10.1016/J.CONBUILDMAT.2023.130504.

2 Literature Review

The corrosion of reinforcing steel is one of the most critical mechanisms of concrete deterioration, posing a severe threat to the durability and structural integrity of the RC structures. Corrosion generates expansive pressure against the surrounding concrete as corrosion products accumulate around the reinforcing steel. This pressure induces cracking, spalling, and delamination, ultimately compromising the mechanical properties of the concrete and its capacity to transfer loads effectively (Gonzalez et al., 1996). Globally, corrosion-related damage is a primary cause of structural degradation, leading to significant maintenance costs and eventually premature failure of aging critical infrastructure (Broomfield 2007). Unlike other deterioration internal mechanisms, such as alkali-silica reaction (ASR) or delayed ettringite formation (DEF), which primarily affect the concrete microstructure, corrosion uniquely impacts the bond between steel and concrete, reducing both serviceability and structural capacity (Zhang et al., 2020).

A significant challenge in addressing corrosion-induced deterioration lies in bridging the gap between material-level assessments and their implications for structural performance. Petrographic and microscopic evaluations, along with mechanical testing, provide valuable insights into cracking patterns and damage severity (Sanchez et al., 2018). However, transforming these insights into practical strategies for maintenance and repair requires a detailed understanding of corrosion mechanisms, the factors affecting the evolving rate of these processes (e.g., water-to-cement ratio, concrete cover thickness, and chloride ingress, among others), and the progression of damage over time (Bertolini, 2013; Polder et al., 2014). Such comprehension and quantification of damage are crucial for predicting the residual performance of corroded structures and developing effective rehabilitation strategies.

While internal swelling reactions such as freeze and thaw (FT) and delayed ettringite formation (DEF) primarily affect the cement paste, corrosion of steel reinforcement introduces a dual challenge. This process compromises not only the steel reinforcement but also the surrounding concrete, accelerating structural degradation and diminishing service life. The dual impact emphasizes the urgency of addressing corrosion-induced deterioration as a critical aspect of RC maintenance.

Given the widespread prevalence of reinforcement corrosion in the RC structures globally and its complex interaction with environmental factors, a focused examination of corrosion mechanisms is imperative. This chapter explores key aspects of corrosion-induced deterioration, including current tools for assessing and measuring damage, emphasizing cracking induced by corrosion. Special attention is given to the current version of the DRI(Sanchez 2024), a promising protocol for quantifying damage extent. By addressing these elements, the review aims to identify gaps in existing knowledge and support the advancement of targeted, reliable assessment techniques for corrosion-induced concrete damage.

2.1 Corrosion in Reinforced Concrete

Reinforcing steel bars in concrete typically do not corrode. However, concrete, being porous and retaining moisture and air within its pores, can facilitate steel corrosion in the presence of both air and water. This apparent contradiction is explained by the fact that concrete is inherently alkaline. The microscopic pores in concrete contain elevated levels of soluble calcium, sodium, and potassium oxides. During the hydration process, these oxides react with water to form hydroxides, including calcium hydroxide [$Ca(OH)_2$], a primary hydration by-product of Portland cement. This combination creates an extremely alkaline environment within the cement paste matrix, with a pH range of 12–13 (Bertolini 2013).

This high alkalinity facilitates the formation of a passive layer on the steel surface, likely composed of a mixture of metal oxide/hydroxide and minerals from the cement. This dense, thin, and impenetrable film serves as a barrier that prevents further corrosion of the steel, if the passivating conditions are maintained (Gonzalez et al., 1996). Depassivation occurs when the concrete cover becomes either carbonated due to the penetration of atmospheric carbon dioxide or contaminated with sufficient quantities of chloride ions.

Reinforcement concrete in the RC structures occurs in two stages: initiation and propagation, as described hereafter.

2.1.1 Corrosion Initiation

The corrosion process in the RC begins with the disruption of the passivating layer. When this protective environment is compromised, due to carbonation or chloride ingress, the passive layer deteriorates, and corrosion is initiated (Broomfield 2007).

Corrosion of reinforcing steel is an electrochemical process. The anodic reaction at the steel surface begins with the dissolution of iron in the concrete's pore water, where iron releases electrons as it transforms into ferrous ions (Fe^{2+}):

Anodic reaction:

$$Fe \rightarrow Fe^{2+} + 2e^{-} \qquad \text{(Equation 2.1)}$$

This reaction generates free electrons ($2e^{-}$) that must be neutralized. To maintain electrical neutrality, a corresponding cathodic reaction occurs, facilitated by the presence of oxygen and water. This reaction consumes the electrons and produces hydroxyl ions (OH^{-}):

Cathodic reaction:

$$2e^{-} + H_2O + \frac{1}{2}O_2 \rightarrow 2OH^{-} \qquad \text{(Equation 2.2)}$$

While these reactions represent only the initial phases of corrosion, understanding this electrochemical pair is crucial, as it underpins the progression of rust formation on steel within concrete (Broomfield 2007).

Soluble ferrous ions (Fe^{2+}), further oxidize to produce, corrosion products, whose accumulation around the reinforcing bar initiate a process of structural degradation.

2.1.2 Corrosion Propagation

Once corrosion initiates, it progresses through additional reactions that create expansive compounds on the steel surface. In the presence of oxygen, ferrous hydroxide [$Fe(OH)_2$] – an

intermediate corrosion product – undergoes further oxidation and transforms into ferric hydroxide [$Fe(OH)_3$] and, eventually, hydrated ferric oxide (rust):

Formation of Ferrous Hydroxide:

$$Fe^{2+} + 2OH^- \rightarrow Fe(OH)_2 \qquad \text{(Equation 2.3)}$$

Conversion to Ferric Hydroxide and rust:

$$4Fe(OH)_2 + O_2 + 2H_2O \rightarrow 4Fe(OH)_3 \qquad \text{(Equation 2.4)}$$

$$2Fe(OH)_3 \rightarrow Fe_2O_3 \cdot H_2O + 2H_2O \qquad \text{(Equation 2.5)}$$

These reactions are depicted in Figure 2-1 and illustrate how rust (hydrated ferric oxide) accumulates on the steel. The unhydrated ferric oxide occupies roughly twice the volume of the original steel, but with hydration, the volume can expand six to tenfold, Figure 2-2, leading to significant stresses at the steel/concrete interface (Broomfield 2007). This expansion creates substantial internal pressure at the steel-concrete interface, leading to cracks that propagate through the concrete matrix.

As rust forms and expands, tensile stresses are exerted on the surrounding concrete. This pressure results in cracking along the reinforcement, as the concrete cannot accommodate the increased volume without fracturing. Over time, these cracks widen, leading to the detachment, or spalling, of sections of concrete cover from the structure. Spalling exposes more steel to environmental conditions, which in turn accelerates the corrosion process and exacerbates structural deterioration (Broomfield, 2007).

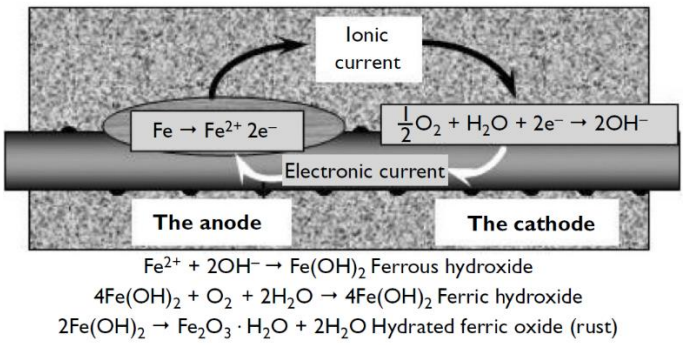

Figure 2-1 - The steel corrosion process, adapted from Broomfield (2007)

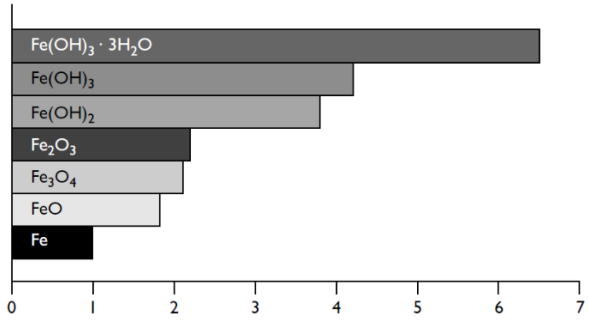

Figure 2-2 - Volume relationships between iron and its oxides according to the corrosion process adapted, from Broomfield (2007)

2.1.3 Corrosion in Concrete: Causes and Mechanisms

In general, reinforcement corrosion in concrete can be triggered by two mechanisms. Firstly, carbonation plays a significant role, wherein the concrete undergoes a reaction with carbon dioxide from the surrounding environment, leading to a decrease in pH levels. Secondly, the presence of chloride ions, whether inherent in the concrete constituents during manufacturing or introduced during the service life through ingress, leads to reinforcement depassivation. These two processes (i.e., concrete carbonation and chloride ion ingress) collectively contribute to the degradation of concrete structures over time.

2.1.3.1 Carbonation-induced corrosion

The focus on concrete carbonation has intensified recently due to increasing concerns about climate change. This naturally occurring corrosion process in the RC structures advances gradually but consistently.

The carbonation process arises from the interaction between atmospheric carbon dioxide and calcium hydroxide in concrete. Carbon dioxide gas dissolves in water, forms carbonic acid (H_2CO_3), and reacts with calcium hydroxide, leading primarily to the precipitation of calcium carbonate ($CaCO_3$), which forms a lining within the concrete pores. These chemical reactions deplete hydroxyl ions (OH^{-1}) in the pore solution, reducing the pore water pH, from above 12.5 to below 9. In this range, the passive layer becomes unstable, potentially enabling general corrosion if there is an ample presence of oxygen and water near the rebar (Zhou et al., 2015). Equations 2.6 and 2.7 show the process of producing calcium carbonate (Broomfield, 2007).

$$CO_2 + H_2O \longrightarrow H_2CO_3 \text{ (carbonic acid)} \qquad \text{(Equation 2.6)}$$

$$H_2CO_3 + Ca(OH)_2 \text{ (pore solution)} \longrightarrow CaCO_3 + 2H_2O \qquad \text{(Equation 2.7)}$$

The risk for carbonation-induced corrosion increases with small concrete covers for the reinforcing steel. Additionally, it may occur even with high covers if the concrete pore structure is open and interconnected forming a network that facilitates the CO_2 ingress.

Figure 2-3 illustrates the ingress and dissolution of atmospheric CO_2 in the concrete cover, causing a mostly uniform carbonation front due to porosity and cracks. This leads to progressive decalcification of Ca-bearing phases and $CaCO_3$ precipitation, reducing the pH below 9 (Rodrigues et al., 2021).

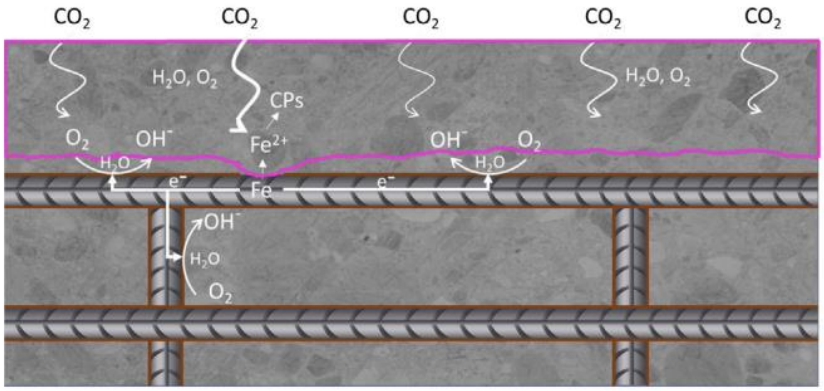

Figure 2-3 - The mechanism of carbonation-induced corrosion in the RC, adapted from Rodrigues et al. (2021)

Upon the carbonation front reaching the rebar, there is local depassivation caused by the dissolution of the passive film at near-neutral pH. This marks the end of the initiation period, accompanied by an increase in the corrosion rate. Subsequently, there is the formation and diffusion of Fe^{2+}, leading to the precipitation of corrosion products (Rodrigues et al., 2021).

2.1.3.2 Chloride-induced corrosion

The existence of chloride ions within concrete may arise from components of aggregates that are contaminated, mixing water that is tainted, or ingress from the surrounding environment. This environmental exposure may occur in a marine setting, involving wetting/drying cycles, or through the utilization of de-icing salts, especially, calcium chloride ($CaCl_2$), magnesium chloride ($MgCl_2$), and sodium chloride (NaCl), during winter.

The infiltration of chloride ions primarily transpires via capillary pores, wherein free chloride ions (Cl^-) are drawn through capillary suction, diffusion, and/or permeation. Consequently, the onset time of corrosion significantly relies on transport factors, especially the diffusion coefficient of overall chloride ions within the concrete. As illustrated in Figure 2-4, the incorporation of chloride ions into the material originates from de-icing agents or exposure to marine surroundings. Non-homogeneous penetration arises because of variation in porosity and crack distribution, with chloride ions forming bonds with hydrated phases. Local depassivation occurs when chloride ions reach the reinforcement in sufficient quantities above the so-called chloride threshold concentration (Rodrigues et al., 2021).

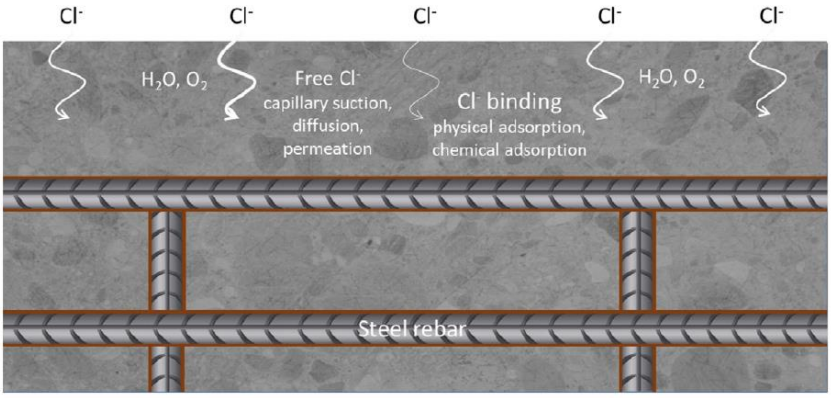

Figure 2-4 - The mechanism of chloride-induced corrosion, adapted from Rodrigues et al. (2021)

There are two scenarios to consider in chloride-induced corrosion. In the case of low chloride content, there is a repeated process of depassivation and repassivation resulting from cathodic protection by the precipitation of corrosion products on the remaining passive layer. On the other hand, in locations with high chloride content, pitting corrosion occurs, leading to the creation and sustenance of an aggressive microenvironment. This distinct mechanism highlights the varied and complex nature of the chloride-induced corrosion processes, as illustrated in Figure 2-5 (Rodrigues et al., 2021).

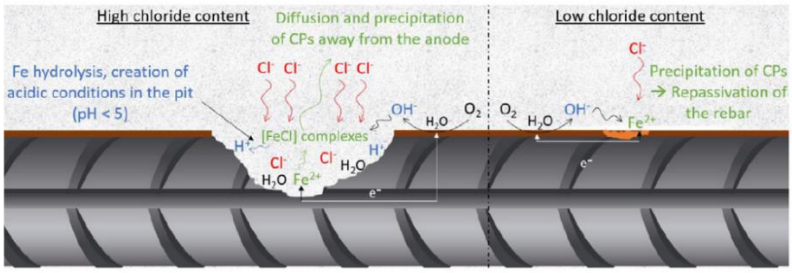

Figure 2-5 - Chloride-induced corrosion: exploring varied outcomes in high and low chloride environments, adapted from Rodrigues et al. (2021)

2.1.1 Corrosion-Induced Damage in the RC

In this study, the term *damage* specifically denotes the quantifiable adverse effects of reinforcement corrosion on the mechanical performance, structural integrity, and durability of an RC element. Corrosion-induced damage is primarily characterized by 1) A reduction in the steel cross-sectional area and ductility; 2) A decline in the bond action between the reinforcement and concrete; and 3) A loss of physical integrity and durability in concrete, largely influenced by internal cracking of concrete induced by corrosion. The discussion in this study is specifically related to corrosion-induced damage in the concrete surrounding steel reinforcement.

The RC structures experience diverse forms of deterioration due to the expansive nature of corrosion products. The oxidation of steel reinforcement results in the formation of rust, which occupies a significantly larger volume than the original steel, generating internal tensile stresses within the concrete. Once these tensile stresses exceed the concrete's inherent tensile strength, cracking initiates. Crack propagation is influenced by multiple factors, including the degree of corrosion, the thickness of the concrete cover, and the tensile properties of the concrete. As corrosion advances, cracks widen, progressively reducing structural stability and facilitating the ingress of aggressive agents, thereby accelerating deterioration (Nepal 2015).

Spalling represents another prominent consequence of reinforcement corrosion. This process results in the detachment of surface layers, thereby exposing the underlying reinforcement to further environmental degradation. The severity of spalling is contingent upon factors such as concrete cover thickness and strength (Moccia et al., 2021).

A further critical effect of reinforcement corrosion is the reduction of the steel's cross-sectional area. Corrosion leads to material loss in the reinforcing steel, diminishing its tensile strength and, consequently, the load-bearing capacity of the structural element. Even minor reductions in steel cross-section can significantly impair the performance of the RC elements, particularly in structures with minimal reinforcement redundancy. Additionally, this loss of steel directly contributes to a reduction in stiffness, affecting the overall structural response (Yu et al., 2024).

The bond strength between steel reinforcement and surrounding concrete is also adversely impacted by corrosion. Initially, the accumulation of rust at the steel-concrete interface may enhance bond strength by increasing frictional resistance. However, as corrosion progresses, bond

strength deteriorates due to cracking, spalling, and delamination of the concrete cover, ultimately impairing load transfer between steel and concrete. The progressive loss of bond integrity further compromises structural stability, particularly in the RC members subjected to cyclic or sustained loading(Mak et al., 2019).

2.2 Assessment Tools for Corrosion-Induced Cracking in RC

Cracking in the RC structures can be evaluated using a range of non-destructive and microscopic techniques. These methods provide insights into the initiation, progression, and extent of cracking, enabling engineers and researchers to assess structural integrity and predict long-term deterioration. Most condition assessment techniques focus on external cracking, designed for surface-level inspections of structural evaluations, while a few techniques are applied to appraise the internal condition of affected concrete. The following sections outline key assessment tools used for evaluating damage in concrete, starting with visual inspections, non-destructive methods usually used to aid visual inspection, and thus discussing the tools currently used to apprise internal conditions.

2.1.4 Manual and Visual Assessment of Cracking

Manual measurement and visual assessment are fundamental methods for evaluating corrosion-induced cracking in the RC structures. These approaches involve direct observation and recording of observable crack characteristics using basic tools such as crack width gauges, calipers, and rulers. They enable engineers to assess critical crack parameters, including width, length, and depth, particularly in accessible areas of the concrete surface. While straightforward and cost-effective, these methods provide valuable baseline data for understanding the extent of deterioration, making them particularly useful in preliminary assessments (Gonthina et al., 2023; Neville, 1996).

Manual measurement is advantageous due to its simplicity and affordability, as it does not require sophisticated equipment or extensive training. However, its accuracy and consistency depend significantly on the operator's skill and judgment. Additionally, it is unsuitable for assessing subsurface cracks or very fine openings that are difficult to detect visually (ACI Committee 224,

2007). Despite these limitations, manual measurement remains a crucial tool in early-stage crack assessment, often serving as a preliminary step before employing more advanced techniques.

Visual inspection, allows for the direct observation of visible surface damage, including crack formation, rust stains, and spalling. This method is particularly effective in identifying early signs of corrosion-induced damage. As an initial step in structural evaluations, visual inspection provides immediate qualitative data without requiring sophisticated equipment. However, its reliability is constrained by its inability to detect subsurface or early-stage corrosion damage, which may not yet be visible on the surface (Berrocal et al., 2022).

To enhance the accuracy of visual assessments, studies emphasize supplementing visual inspection with non-destructive techniques. For instance, integrating Infrared Thermography (IRT) or Digital Image Correlation (DIC) provides more precise external crack width measurements and enables continuous monitoring of crack propagation. Such complementary tools are particularly beneficial in laboratory studies and long-term structural monitoring, where visual inspection alone may not sufficiently capture the detailed progression of corrosion-induced cracks (Pfändler et al., 2022).

Despite its limitations, visual inspection remains the primary assessment approach for corrosion-induced cracks, especially in field settings where more advanced methods may not always be feasible. When integrated with advanced techniques capable of capturing both external and internal damage, visual assessment becomes a fundamental component of a comprehensive corrosion evaluation strategy (Berrocal et al., 2022; Guzmán-Torres et al., 2023).

2.1.5 Infrared Thermography (IRT)

Infrared thermography (IRT) is a non-destructive testing (NDT) method that works by detecting variations in surface temperature caused by underlying defects such as cracks, delamination, or voids. Since cracks alter the thermal properties of concrete, the areas around these defects exhibit different thermal behavior compared to intact regions, making them visible using infrared cameras.

IRT can be applied in two modes: passive and active. In the passive mode, naturally occurring heat, such as sunlight, is used to create thermal gradients across the structure. Active thermography, on the other hand, involves artificially heating the structure and observing the

thermal response. Both approaches allow for the identification of surface-level and subsurface cracks, which can disrupt the thermal conductivity of the concrete (Rocha and Póvoas 2019).

Infrared thermography is effective in detecting early signs of cracking, but it has some limitations. Its accuracy depends heavily on environmental conditions, such as temperature gradients and sunlight exposure. Studies have shown that the method is more effective during early morning or after sunset when temperature differences between damaged and intact areas are more pronounced. However, in cases of advanced deterioration, thermography alone may not provide sufficient depth information about cracking, making it necessary to combine it with other techniques, such as those based on ultrasound wave propagation, to enhance accuracy (Milovanović and Pečur 2016). Overall, IRT offers a quick and non-invasive way to detect and monitor corrosion-related cracks, making it a valuable tool for regular inspection of large structures. However, to fully understand the extent of the damage, it is often used in combination with other methods that can provide more precise data about crack depth and the internal state of the concrete.

2.1.6 Digital Image Correlation (DIC)

Digital Image Correlation (DIC) is a powerful, non-contact optical technique widely used for measuring surface displacements and strains in materials, particularly for assessing structural behavior under various loads. In the context of the RC structures, DIC has been proven highly effective for detecting and analyzing crack formation and progression (Pan 2009). By capturing a sequence of images of a specimen's surface and correlating them, DIC provides detailed full-field strain and displacement measurements. This allows for the identification of crack initiation points, monitoring of crack growth, and the assessment of surface deformation in real-time (Pan 2009).

A key advantage of DIC is its ability to measure strain distribution across an entire surface, unlike strain gauges, which capture data at discrete points. As a non-invasive technique, it is ideal for studying fragile or degrading structures. While traditionally limited to laboratories, advancements in portable systems now enable field applications, such as monitoring crack propagation in bridges and retaining walls (Aryanto et al., 2023; Mousa et al., 2023). These developments highlight its potential for non-invasive assessments of reinforced concrete structures in both research and practical engineering contexts.

Recent studies have highlighted the utility of DIC in measuring crack width, crack propagation speed, and surface strain distribution, providing highly accurate and detailed insights into the corrosion process (Pan 2009). DIC has been used to track the development of corrosion-induced cracks in concrete beams, where it can provide data on both the location and size of the cracks (Michel Kuntz 2011). This capability makes it an invaluable tool for understanding the mechanical behavior of concrete structures under stress and for developing maintenance strategies to prevent failure (Mousa et al., 2023).

2.1.7 Ultrasonic Pulse Velocity (UPV)

Ultrasonic Pulse Velocity (UPV) is a widely used non-destructive testing (NDT) method for assessing the internal condition of concrete structures. UPV works by measuring the time it takes for ultrasonic pulses to travel through a material. In concrete, the pulse velocity decreases in areas with cracks or voids.

A lower velocity reading typically indicates areas where cracks, voids, or other forms of deterioration have occurred. This method is sensitive enough to detect both surface-level and deeper internal cracks that may not be visible during surface inspections (Ongpeng 2017).

The method is non-invasive, making it particularly useful for ongoing monitoring of the RC structures in both laboratory and field settings. However, the effectiveness of UPV can be influenced by factors such as the presence of reinforcement, aggregate size, and the moisture content of the concrete, requiring careful calibration for accurate results (Ongpeng 2017).

2.1.8 Impact Echo (IE)

Impact Echo (IE) testing is an NDT method that uses stress waves to detect internal cracks and delamination in concrete structures. This technique works by generating low-frequency stress waves through a small impact on the concrete surface. These waves travel through the material and reflect upon encountering defects, such as cracks or voids. By analyzing the frequency of the reflected waves, IE testing can provide insights into the location, depth, and extent of internal anomalies (Mary Sansalone 1997).

IE testing is particularly effective for assessing subsurface cracks induced by corrosion, such as concrete cover delamination. These corrosion-induced cracks may not be visible on the surface, but IE testing can reveal their presence by identifying changes in wave frequencies that indicate areas of internal damage. This makes IE testing highly valuable for evaluating corrosion damage that compromises structural integrity without any outwardly visible signs (Sansalone 1997).

One of the primary advantages of IE testing is its ability to assess the depth and progression of cracks. The technique is also highly versatile, applicable to both field and laboratory settings, and can be used on various concrete elements, including slabs, walls, and bridge decks. However, IE testing requires skilled operators and specialized equipment to interpret the results accurately. For the most comprehensive assessment, IE testing is often combined with other NDT methods, such as Ground Penetrating Radar (GPR) or Ultrasonic Pulse Velocity (UPV), which further enhance its accuracy and provide additional insights into the condition of the concrete (Bungey 2006).

2.1.9 Acoustic Emission (AE)

Acoustic Emission (AE) is a highly effective non-destructive technique for detecting and monitoring cracking in the RC. AE works by capturing elastic waves generated by the release of energy during crack formation and propagation. These waves are recorded by sensors placed on the surface of the concrete, and the location and intensity of the emissions help in assessing the severity of the damage.

AE can detect the onset of cracking, monitor crack growth, and track structural degradation in real-time. The technique's non-invasive nature, combined with its ability to capture dynamic events, makes it well-suited for both laboratories testing and in-situ applications on large concrete structures (Barbosh et al., 2022). However, AE requires sophisticated signal processing methods, such as wavelet transforms, to accurately filter out noise and interpret the data effectively (Barbosh et al. 2022; Skarżyński et al., 2022).

In the context of corrosion-induced cracking, AE has proven to be valuable for characterizing both the initiation and progression of cracks, which are critical for assessing the structural health of the RC under corrosive environments (Ohtsu et al. 2010).

2.1.10 Ground Penetration Radar (GPR)

Ground Penetrating Radar (GPR) is an NDT technique widely used to detect internal defects in concrete, rather than general structural deficiencies. GPR operates by emitting high-frequency electromagnetic waves into the concrete structure; these waves reflect upon encountering interfaces between materials, such as cracks or embedded steel reinforcement. Variations in the reflected signals provide valuable data on the presence and location of cracks (Solla et al., 2012).

One limitation of GPR in corrosion-specific applications is that its effectiveness can be influenced by factors such as concrete moisture and chloride content, which are often present in corroded concrete environments (Sengul2008). These factors can attenuate the electromagnetic signal. Additionally, GPR requires expert interpretation, as overlapping defects can complicate the analysis, highlighting the need to combine it with complementary methods like Impact Echo (IE) or Ultrasonic Pulse Velocity (UPV) to confirm the presence of cracking (Łaziński et al., 2024).

GPR provides a fast, non-invasive way to identify corrosion-induced cracking in RC structures. Its ability to detect early-stage cracks near reinforcement makes it particularly valuable for regular inspections of large structures, helping to target potential issues related specifically to corrosion rather than other concrete deficiencies. Combining GPR with additional NDT methods allows for a more accurate understanding of the structural impact of corrosion-induced cracking (Faris et al., 2023).

2.1.11 X-ray Computed Tomography (CT)

X-ray Computed Tomography (CT) Scanning is an advanced non-destructive testing method used to visualize and quantify internal cracks and other forms of damage in the RC structures. This technique produces detailed cross-sectional images of a specimen, which are reconstructed into three-dimensional models, enabling researchers to assess the internal condition of concrete without physically cutting into the material. While X-ray CT is predominantly used in laboratory settings due to its need for controlled conditions and specialized equipment, there is growing interest in its application in the field.

Recent advancements in portable and mobile CT systems have enabled limited field use, particularly for assessing critical infrastructure components, such as bridge decks and nuclear plant structures, where high-resolution internal imaging is essential (Grzesiak, 2023). However, challenges such as equipment size, resolution limitations, and environmental interferences currently restrict its widespread adoption outside laboratory environments (Landis 2010).

CT scanning is particularly useful in the context of corrosion-induced damage, where it provides a high-resolution view of cracks, voids, and the distribution of corrosion products around the steel reinforcement (França de Mendonça Filho et al., 2021). For example, studies such as the one conducted by Han et al. (2023) have demonstrated the utility of CT scanning for visualizing corrosion-induced cracking and void formation in reinforced concrete. By capturing differences in material densities, such as between steel rebar, corrosion products, concrete matrix, and pores, CT images allow precise identification and quantification of damage phases, including crack propagation and internal void formation.

Recent research has utilized 4D CT imaging, which adds the dimension of time to capture the evolution of corrosion-related damage, offering insights into the dynamic process of crack formation and growth. Through advanced software, the pore structure and phase segmentation of the concrete can be analyzed, allowing for a more quantitative understanding of how corrosion affects the internal structure. This makes CT scanning an invaluable tool for long-term monitoring of the RC's structural health (Taheri-Shakib 2023).

2.1.12 Petrographic Analysis as a Basis for Quantifying Concrete Durability

Visual inspection (VI) methods, including qualitative descriptions of external cracking, along with NDT, provide an initial assessment of concrete surface damage. These techniques offer a preliminary understanding of the material’s condition, while advanced techniques such as CT-scan, complement such understanding, providing information on the microstructure condition of the material. However, the techniques discussed are limited in connecting their measurements with the current condition of deterioration (i.e., extent of damage), which is one of the important questions related to condition assessment of critical concrete infrastructure. To address this limitation, microscopy techniques, both qualitative and quantitative, have been used to assess

deterioration of concrete caused by internal mechanisms. These methods not only enhance the understanding of deterioration processes, such as internal swelling reactions (ISR), but also provide a more comprehensive evaluation of the extent and severity of damage within the affected concrete.

Petrographic analysis involves the microscopic examination of thin or polished sections of concrete, providing valuable insight into its microstructure. This technique enables the identification of key characteristics, including aggregate mineralogy, different phases of cement hydration, and secondary reaction products. Historically, petrography has been a fundamental tool in concrete research, particularly for assessing the condition of deteriorated concrete (Jana 2005). Over time, its application has expanded across the concrete construction industry, where it serves multiple purposes. Additionally, petrographic examination functions as a quality control measure, aiding in detecting errors in proportioning, mixing, placement, finishing, or curing concrete, as outlined in ASTM C856-20 (2020). Beyond quality assessment, petrography is instrumental in diagnosing the causes of concrete deterioration, whether due to chemical attacks, including acid, alkali-silica reaction, sulphate, chloride, or seawater exposure, or physical stressors such as freeze and thaw and fire damage (Erlin 1990; Poole 2016). Furthermore, it contributes to evaluating the effectiveness of rehabilitation and repair strategies by assessing the performance of repair materials and their compatibility with the existing concrete (Sanchez, 2024).

Studies have shown that petrographic distress features observed at the mesoscale can reliably correlate with macrostructural performance when compared with standardized mechanical and durability testing methods (Sanchez, 2024; Martin et al., 2017; Sanchez et al., 2018). Additionally, the mesoscale level identifies distinct damage patterns associated with specific deterioration mechanisms. This not only facilitates the detection of the underlying causes of damage but also enhances the understanding of their potential effects on the engineering properties and long-term durability of concrete.

Several petrographic protocols have been developed at the mesoscale over recent decades to address the need for a systematic assessment of concrete damage. Among these, the Damage Rating Index (DRI), a semi-quantitative petrographic method, and image analysis, a fully quantitative approach, has proven to be among the most effective techniques. Additionally,

emerging technologies continue to advance the ability to quantitatively evaluate internal-induced deterioration in concrete, providing more precise and comprehensive assessments of damage mechanisms (Sanchez, 2024).

2.3 Damage Rating Index (DRI)

The Damage Rating Index (DRI) was developed by Grattan-Bellew of the National Research Council of Canada, based on the work of Sims (1992) The method was initially designed for the study of the Saunders Power Station (Ontario, Canada), which exhibited signs of alkali-aggregate reaction (AAR). It involves counting the presence of petrographic indicators of AAR on cut and polished surfaces of concrete cores. Concrete cores with a minimum diameter of 100 mm are typically preferred, as they allow for the examination of surfaces at least 150 cm^2 in size. If the aggregate is large (over 100 mm), a 150 mm diameter core ensures the observation of a representative surface (Grattan-Bellew; A. Danay 1992).

The Damage Rating Index is calculated by counting AAR-related petrographic indicators within 1.5 cm grid squares under a stereomicroscope at 16x magnification (Table 2-1). The sum of each indicator is then multiplied by weighting factors, arbitrarily assigned to reflect their relative contribution to AAR-induced damage (Table 2-1). The total weighted score, normalized to 100 cm^2, gives the Damage Rating Index.

At the Saunders Power Station, results showed significant variation between samples, attributed to low moisture content (drying) in thinner elements or differences in aggregate reactivity within the structure. Concrete less exposed to moisture exhibited lower DRI values. The method's reproducibility was evaluated by analyzing two cores from the same section, yielding a 5% difference in DRI, which was considered highly satisfactory.

Originally developed for assessing damaged dam concrete, the DRI was later applied by Shrimer (2006) to smaller-scale structures. The method revealed significant variability in AAR extent across different structural sections. For example, samples from a retaining wall along the Goderich River (Ontario) showed higher DRI values near the concrete surface than at greater depths, aligning with prior petrographic observations. The DRI was also applied to a pier in Vancouver's port, where internal cracking was far more severe (reaching disaggregated concrete) than surface observations suggested, for reasons that were not immediately clear. However,

the external appearance of the concrete corresponded well to DRI values obtained from other samples.

Over the years, modifications have been made to the DRI method, such as reducing the observation field size to 1 cm² or adjusting weighting factors (Table 2-1) Shrimer (2006) proposed increasing the weighting for closed cracks and debonded aggregates, while introducing two new factors: corroded particles (factor of 3.0) and freeze-thaw cracks propagating through paste and aggregates (factor of 4.0). Meanwhile, Clemeña et al. (2000); developed a variation called Petrographic Damage Rating, based on the DRI but performed at 50x magnification, using smaller observation fields (1.5 x 2.0 mm) (Table 2-1). The weighting factors applied by different researchers can vary significantly from the original method proposed by Grattan-Bellew.

Table 2-1 - DRI weighing factors first implemented, Adapted from Clemeña et al. (2000); P.E. Grattan-Bellew; A. Danay (1992); Shrimer (2006); Sims (1992)

`	Weighing factor			
Crack in the aggregate particle	0.25	-	2.0	0.5
Closed crack in the aggregate particle	-	0.75	-	-
Open crack in the aggregate particle	-	4.0	-	-
Crack with gel in the aggregate particle	2.0	2.0	4.0	2.0
Coarse aggregate debonded	3.0	3.0	0.5	4.0
Reaction rims around aggregate particles	0.5	0.5	4.0	0.5
Crack in the cement paste	2.0	2.0	4.0	2.0
Crack with reaction product in the cement paste	-	-	-	4.0
Disaggregated/corroded aggregate particle	-	-	4.0	3.0
Area of induvial squares in the DRI	1.5 (cm²)	1.0 (cm²)	1.5 x 2.0 (mm)	1.0 (cm²)
Magnification	15-16x	15-16x	50x	15-16x

The most recent version of DRI was modified by Sanchez et al. (2015) and Villeneuve (2011), establishing the features of deterioration related to internal swelling reaction mechanisms and adjusting the weighting factors, obtaining 20% variability among operators in an intra-laboratory program. The current types of deterioration features and their ultimate respective weighting factors are thoroughly presented hereafter. Finally, Sanchez et al. have adopted the method to assess ASR

damage originating in fine-reactive aggregates, adjusting the size of cracks counted to 1mm, along with the validation of the DRI to assess distress caused by other mechanisms, such as delayed ettringite formation (DEF) and freeze and thaw (FT) in single and combined fashions. Furthermore, Sanchez et al. have developed an extended version of the DRI, which helps understand the deterioration process. The developments above showed the important connection between the DRI outcomes and the mechanical properties of deteriorated concrete (Sanchez et al. 2015, 2016, 2017, 2018).

2.3.1 DRI Protocol

The magnification level (i.e., 15-16x) used in the current version of the Damage Rating Index (DRI) was selected to ensure clear visibility of deterioration features while maintaining correlation with mechanical property loss and the overall extent of damage. This magnification also allows a 1 cm^2 square to fit within the field of view.

The current weighting factors (Table 2-2) were recalibrated to improve the assessment of internal deterioration of concrete. These recalibrations considered that damage within aggregate particles has a lesser impact on mechanical properties than damage in the cement paste, based on concrete failure mechanisms under axial loading. The current version of DRI enhances correlation between DRI results, expansion, and mechanical property reduction, while also improving inter-operator consistency.

Diagnosis using DRI considers: i) Cause identification and estimation – this involves analyzing cracking patterns, crack types, and the presence or absence of secondary products, which provide insights into the underlying deterioration mechanisms; ii) Extent of deterioration estimation – the DRI method quantifies deterioration by counting damage features within 1 cm^2 polished sample grids. Since cracks spanning multiple squares are counted more than once, the method inherently accounts for crack length and propagation. This makes DRI sensitive to damage progression, reinforcing its quantitative nature and representativeness of deterioration severity. The length of cracks (reflected in repeated counts) and assigned weighting factors are key elements of the method (Sanchez et al., 2015). The extent of the deterioration can be further assessed through the extended version of the DRI.

2.3.1.1 Samples Preparation for DRI

The preparation of samples for the DRI procedure involves straightforward steps commonly employed in microscopy. A concrete core or specimen is first cut longitudinally using a masonry saw with a diamond blade, which can be either notched or unnotched. The saw may utilize a water kit or other coolants, such as paraffin oil or kerosene, though caution must be exercised when using non-water coolants, and all safety protocols must be strictly adhered to. It is recommended to complete the cut in a single motion to minimize deep saw marks on the final surface (Figure 2-6).

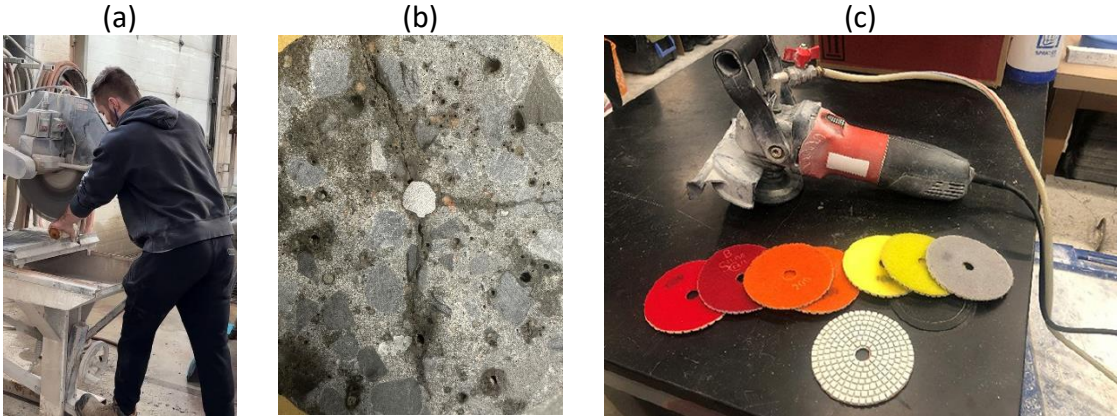

Figure 2-6 - (a) DRI sample cutting (b) sample before grinding (c) handheld polisher

Eighteen-inch lapping disks mounted on a mechanically rotating wheel, or a handheld mechanical polisher, are typically used for the grinding and polishing process. Alternatively, a glass plate can be utilized, onto which abrasive powders are spread and mixed with a lubricant, such as water, to create a grinding or polishing paste. This paste is applied manually using random circular motions with moderate pressure, ensuring the entire surface is evenly ground or polished. The duration of each step depends on the equipment or method employed and the specific materials present in the concrete. After each stage, the surface is cleaned with a soft bristle brush or compressed air to remove slurry, loose abrasives, or dislodged aggregate and cement paste fragments.

To assess the surface quality after each step, sunlight or indoor lighting can be reflected onto the surface to identify areas lacking reflectiveness, often appearing duller or whiter. Any deep scratches or marks from earlier stages should be removed before advancing to the polishing phase. Marks from previous steps should become progressively less visible as the surface is prepared for

subsequent stages. If aggregates appear scuffed during polishing with impregnated disks, additional lubricant, such as water, may be necessary to ensure a smoother finish.

Once the surface achieves a highly reflective finish suitable for analysis, a grid of 1×1 cm squares is marked using a fine-tip permanent marker. Alternatively, a 3D-printed grid or a stiff gardening mesh with a 1 cm by 1 cm grid can be placed on the surface (Figure 2-7), to delineate the sections for analysis. These grids provide a structured framework for systematic examination and ensure consistency in the analysis process (Sanchez, 2024).

Figure 2-7 - (a) A well-polished, highly reflective surface featuring a grid, with visible light reflection in the bottom-right corner (b) a 3D-printed grid positioned over the polished surface, adapted from Sanchez, (2024)

2.3.1.2 Classification of Features of Deterioration

Seven damage features are classified using the DRI. These features or cracks are weighted depending on their relevance to the mechanism(s) under consideration.

Table 2-2 presents the current types of deterioration features and their ultimate respective weighting factors.

Table 2-2 - Types of deterioration features and current weighting factors of the DRI

Type of deterioration feature	Description	Group	Weighting factor
Closed crack in the aggregate particles (CCA)	Tiny crack presenting no opening/gap nor secondary products under 15-16x magnification. Such deterioration feature pre-exists in aggregate particles prior to their incorporation into concrete,	I	0.25

	commonly originating from natural erosion or the aggregate's production stages such as blasting, crushing, and sieving. It is important to note that the natural interfaces between crystals in coarse-grained aggregates are not to be classified as "closed/line" cracks.		
Opened crack or fine network of cracks within the aggregate particle (OCA)	A space (gap) visible under 15-16x magnification. This type of deterioration feature encompasses densely packed / closely spaced tiny branches forming part of an overall cracking network, which often suggests a more progressed stage of reaction or expansion.	II	2
Crack within the aggregate particle, filled with reaction product (OCA_RP)	A gap visible under 15-16x magnification totally or partially filled with secondary products. Such secondary products can originate from a range of mechanisms, such as alkali-silica reaction, internal sulfate attacks (i.e., ettringite and thaumasite), calcium hydroxide and gypsum. It is recommended to characterize their chemical composition through X-ray diffraction (XRD), and/or scanning electron microscopy (SEM) aided with electron energy dispersive X-ray spectroscopy (EDX).	II	2
Disaggregate/corroded aggregate particle (DAP)	An aggregate particle exhibiting evidence of disintegration, characterized by the breakdown into loose rock grains or a general deterioration in its structural integrity.	II	2
Crack in the cement paste (CCP)	A gap (opening) visible in the cement paste under 15-16x magnification, presenting no secondary product.	III	3
Crack in the cement paste filled with reaction product (CCP_RP)	A gap (opening) visible in the cement paste under 15-16x magnification, partially or totally filled with secondary product. It is recommended to characterize their chemical composition through X-ray diffraction (XRD), scanning electron microscopy (SEM) aided with electron energy dispersive X-ray spectroscopy (EDX).	III	3

Debonded aggregate (CAD)	The weakening of the bond between the cement paste and aggregate particles due to a crack (which may be open or partially/fully filled with secondary products) that is present along a substantial part of the interface between the aggregate particle and the cement paste.	-	3

2.3.1.2.1. Closed or line cracks in aggregate particles

A "closed" or line crack (Figure 2-8), typically originates during aggregate processing in quarries, such as blasting, crushing, or sieving, or through natural weathering processes affecting rocks in their natural environment, forming before the aggregate is incorporated into the concrete. At the magnification used in the DRI test (~15x), these cracks lack visible openings and may not appear as significant voids. In cases of alkali-silica reaction (ASR), pre-existing closed cracks can act as preferential pathways for pore solution penetration, internal attack within reactive particles, and the accumulation of reaction products. It is essential to count only clearly visible cracks during the DRI assessment, while taking necessary precautions. Grain joints should not be mistaken for cracks, and cracks that intersect the polishing plane at an angle may create a whitish illumination effect due to optical phenomena, potentially mimicking the presence of reaction products. Careful differentiation is required to ensure accurate identification and assessment (Fournier et al., 2015).

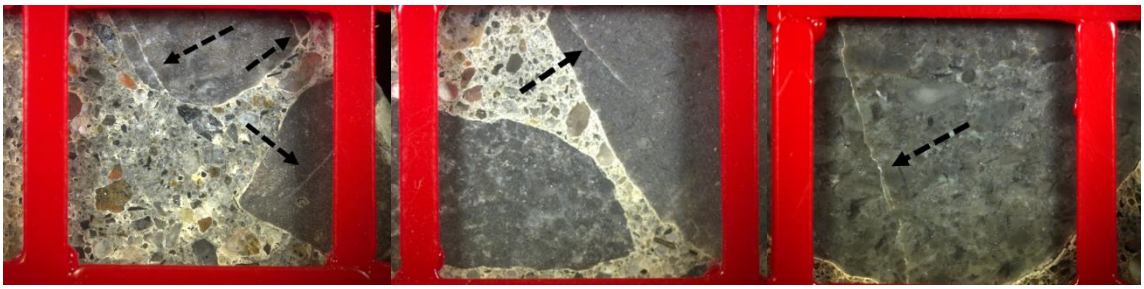

Figure 2-8 - Closed cracks in the aggregate particles

2.3.1.2.2. Open crack in the aggregate

Opened cracks (Figure 2-9), are identified by the clear perception of an opening at the magnification used in the DRI test (~15x). Cracks forming a fine network or creating a larger "diffuse" zone, as opposed to a simple linear feature, are classified as open cracks. These represent

a relatively dense network of cracks that are considered collectively rather than attempting to count each individual component within the network. Such cracking is most likely attributed to active reaction and expansion sites. Fine network cracking is frequently observed in aggregate particles from concrete specimens exposed to laboratory testing conditions, such as elevated temperatures (e.g., 38°C or 60°C) and high relative humidity (100% R.H) (Fournier et al., 2015).

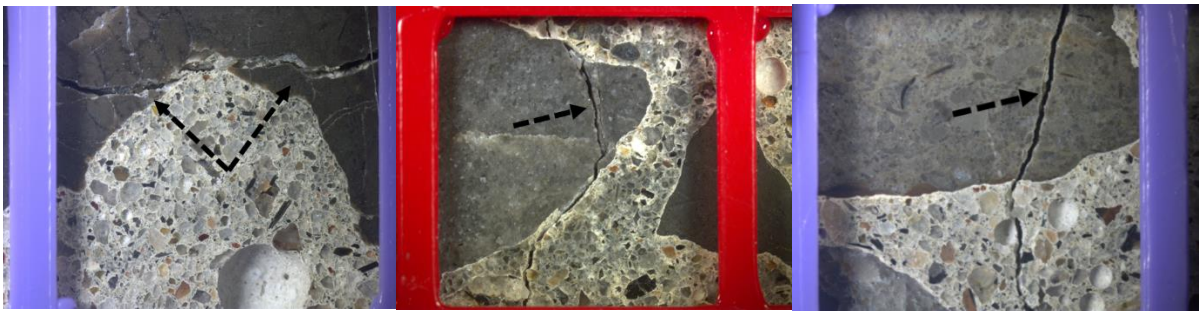

Figure 2-9 - Open cracks in the aggregate particles

2.3.1.2.3. Open crack in the aggregate with reaction products

Certain cracks contain secondary deposits, which may not be continuously present and are often absent in some sections, possibly due to leaching during sample processing. Despite being only partially filled, these cracks are still categorized as containing reaction products (Figure 2-10). In the case of alkali-silica reaction (ASR), the reaction product is often an alkali-silica gel, which may exhibit a vitreous appearance or a whitish, chalky, or powdery texture when in a microcrystalline form (Fournier et al., 2015).

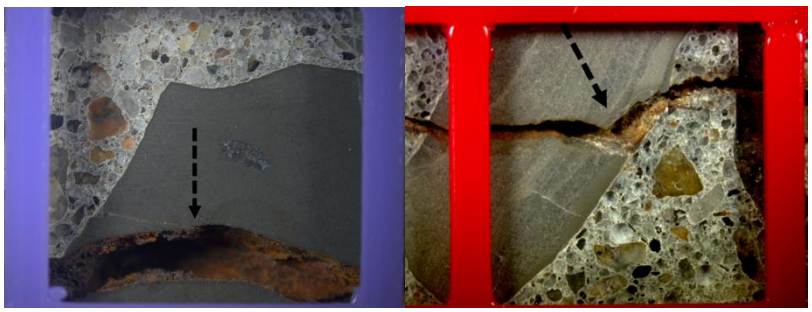

Figure 2-10 - Open cracks in the aggregate particles with reaction products

2.3.1.2.4. Cracks in cement paste

Cracks in the cement paste are categorized into two types: those without reaction products (Figure 2-11) and those with reaction products (Figure 2-12). Certain cracks in the cement paste link multiple aggregate particles (Fournier et al., 2015).

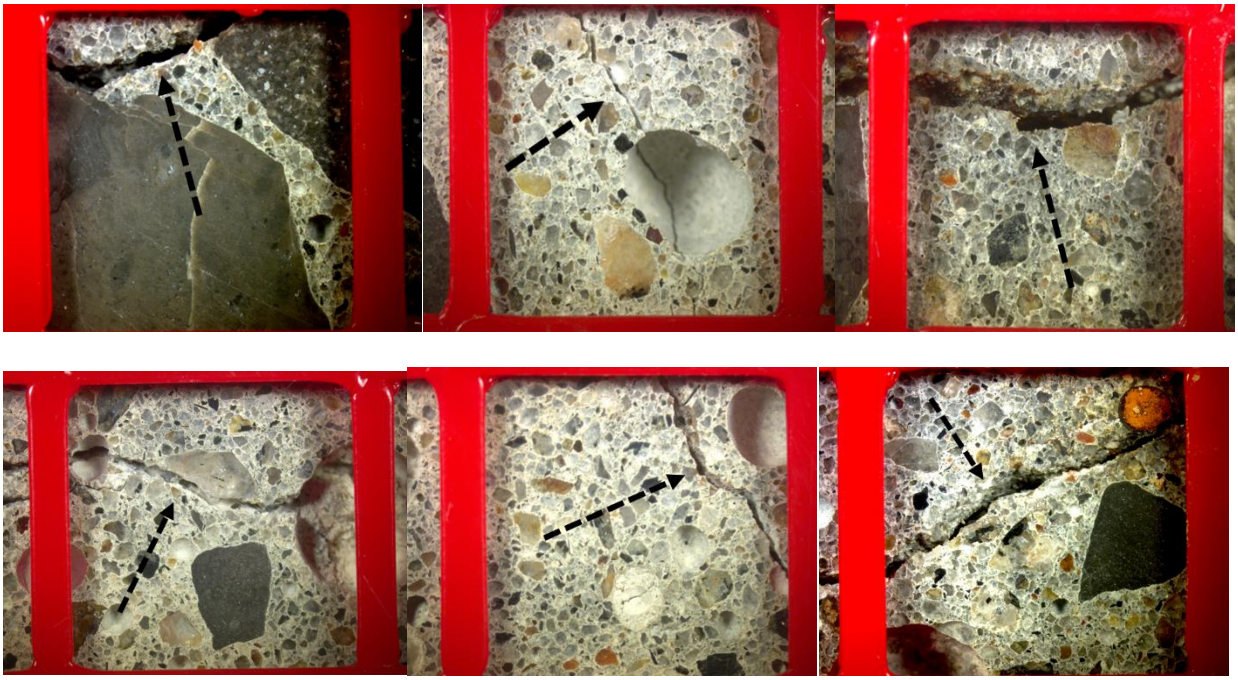

Figure 2-11 - Cracks in the cement paste without reaction products

Figure 2-12 - Cracks in the cement paste with reaction products

2.3.1.2.5. De-bonded aggregate

An aggregate particle is classified as debonded (Figure 2-13), rather than merely exhibiting a crack in the cement paste along its boundary, when the crack is significant enough to likely cause at least

partial separation of the particle during mechanical testing. At least one side of the particle must exhibit separation due to an open crack. If the debonded area contains reaction products, this should be documented accordingly (Fournier et al., 2015).

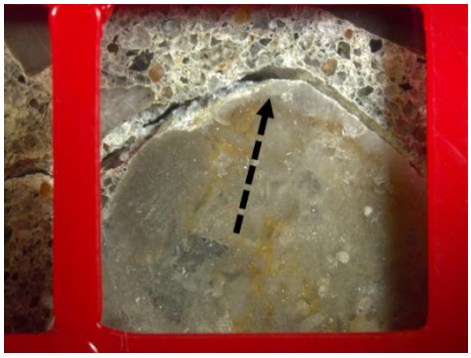

Figure 2-13 - Debonded aggregate particles

2.3.1.2.6. Disaggregated particle

This feature represents the physical manifestation of a reaction leading to the damage or disintegration of an aggregate particle, extending beyond the mere presence of cracks within the particle. It is frequently observed in specific rock types, such as quartzitic sandstone, certain cherts or flints, and some opal-bearing rocks (e.g., shale or sandstone). The identification of these reacted zones is facilitated by the stereomicroscope, which offers enhanced depth of field for clearer observation (Fournier et al., 2015).

2.3.1.3 Extended Version of the DRI

In addition to the conventional DRI method, Sanchez et al., (2015, 2016) introduced an extended version of the DRI, incorporating supplementary petrographic analyses to enhance the assessment of ASR-induced damage. This "extended DRI version" evaluates the microscopic distress features in both absolute counts and relative percentages, without applying weighting factors. This approach provides a more comprehensive understanding of the progression of ASR-induced deterioration in affected concrete.

A key advantage of the extended DRI is its ability to calculate crack density (CD), which quantifies the total number of open cracks in aggregates and cement paste, regardless of the presence of

reaction products. This metric offers additional insight into the overall damage severity within the system.

2.4 Critical Evaluation of DRI Methodology through Literature Analysis

This section reviews key studies that have applied the DRI to evaluate alkali-silica reaction (ASR) in concrete, emphasizing its effectiveness in quantifying ASR-induced damage. While the primary focus of this thesis is to assess the reliability of the DRI as a tool for evaluating corrosion-induced damage in the RC, examining the evolution, application, and refinement of the DRI methodology within the context of ASR offers valuable insights into its adaptability for other deterioration mechanisms. By analyzing research across diverse contexts, this section explores how DRI has been utilized to enhance our understanding of damage mechanisms and to establish reliable, reproducible frameworks for concrete durability assessments. Following the review, the research gap concerning the application of DRI to corrosion-induced damage will be identified, forming the basis for the investigation undertaken in this study.

(Sanchez et al., 2016) investigated the correlation between the DRI and expansion levels caused by ASR in concrete mixes with varying compressive strengths of 25 MPa, 35 MPa, and 45 MPa. The study underscores the reliability of DRI in correlating distress levels to ASR-induced expansion, offering insights into the mechanisms driving damage progression. While DRI has proven effective in laboratory conditions, its application to field-extracted cores highlights both its strengths and limitations.

Progression of Cracking and Mechanisms of Damage

Two distinct types of cracks—Type A (sharp cracks) and Type B (peripheral cracks)—were identified in reactive aggregate particles (Figure 2-14), reflecting different pathways of damage development. Type A cracks originate from aggregate processing or natural porous zones, which facilitate the early penetration of pore solutions and accelerate alkali-silica reactions. These cracks can form within the bulk aggregate volume or along specific planes, such as bedding layers in sedimentary rocks. Type B cracks, on the other hand, develop uniformly along aggregate boundaries, creating concentric "onion skin" patterns as pore solution infiltration progresses.

The study traces the evolution of these crack types as ASR-induced expansion increases:

- At low expansions (~0.05%), Type A and Type B cracks are confined to aggregates, with no visible ASR gel at the magnification used. Type A cracks may form preferentially in crushed or layered aggregates due to their inherent characteristics, while Type B cracks result from uniform chemical interactions at the aggregate boundary.
- At moderate expansions (~0.12%), Type A cracks begin extending into the surrounding cement paste, while Type B cracks remain aggregate-bound. At this stage, ASR gel is detected within open cracks in aggregate particles.
- At higher expansions (~0.20%), Type A cracks penetrate deeply into the cement paste, creating connections between aggregates and integrating with the cementitious matrix. Type B cracks may also extend into the interfacial transition zone (ITZ), potentially causing aggregate debonding.
- At very high expansions (≥0.30%), extensive cracking forms a network linking aggregates and the surrounding cement paste. ASR gel becomes abundant in both phases, exacerbating damage and significantly reducing structural integrity.

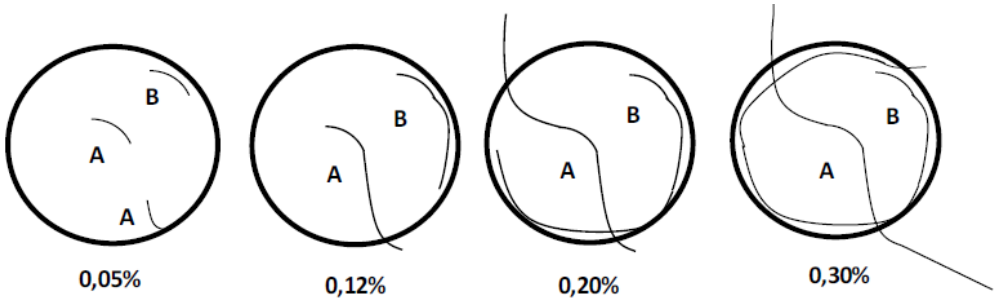

Figure 2-14 - AAR damage model links 0.05–0.30% expansion to Type A (sharp) and Type B (onionskin) cracks adapted, from (Sanchez et al., 2016)

This detailed progression emphasizes the DRI's ability to capture not only the presence of cracks but also their spatial development and interaction with concrete matrices. However, the study critically notes that the grid-based DRI method, which uses 1 cm^2 squares, may over-represent crack frequency due to overlapping counts across adjacent squares. This limitation suggests that

DRI measures both the number and extent of cracks, which may complicate interpretations, particularly at higher expansion levels.

Field Investigation of DRI

The practical utility of DRI was further explored through its application to concrete cores extracted from an ASR-affected overpass in Quebec. These cores exhibited clear distinctions in damage between exposed and non-exposed zones, as well as between surface and internal sections (Figure 2-15). DRI values were consistently higher for exposed surface cores (1075) compared to non-exposed internal cores (700), reflecting the impact of environmental exposure on distress progression. The correlation between field and laboratory findings was notable, with field cores exhibiting damage patterns comparable to laboratory specimens expanded beyond 0.30%.

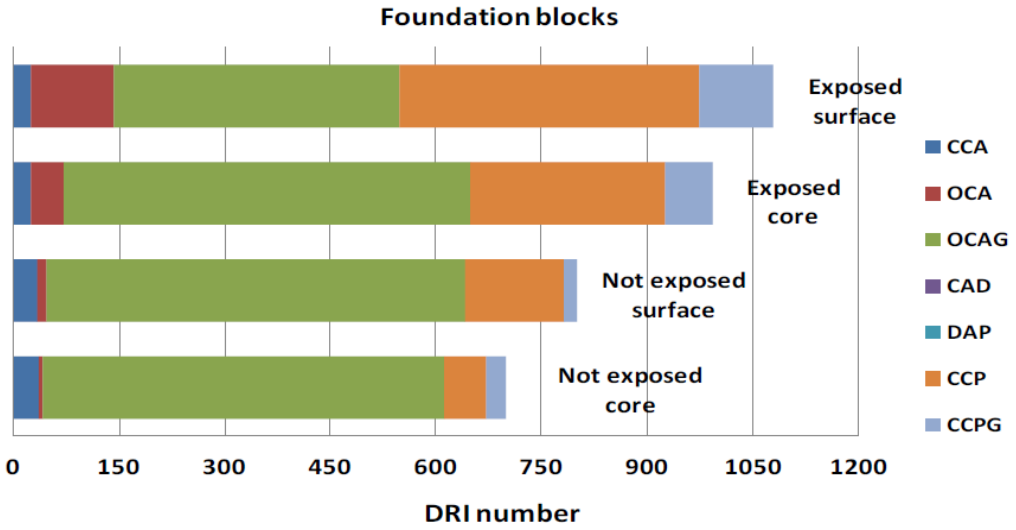

Figure 2-15 - DRI charts, adapted from Sanchez et al. (2016)

This comparison underscores the DRI's potential for field applications but highlights the need for careful consideration of sample representativeness. Field cores are subject to variability in environmental exposure, loading conditions, and structural constraints, which may influence DRI measurements. Despite these challenges, the study found that DRI thresholds established in laboratory settings provided a reasonable benchmark for evaluating field-damaged concrete.

Critical Insights and Practical Implications

While the DRI provides valuable quantitative insights into internal cracking and overall distress, the study raises critical questions about what the index truly measures. The DRI captures both the frequency and extent of cracks, which may include length and width as secondary factors depending on the grid-based counting method. This dual representation of damage complicates direct comparisons with other metrics, such as modulus of elasticity or tensile strength, which focus on specific mechanical properties.

Moreover, the reliance on visual observations and grid-based counting limits the DRI's ability to fully characterize the mechanisms underlying crack formation. For instance, the study notes that Type A and Type B cracks develop differently in aggregates with varying lithologies, yet these nuances may be underrepresented in DRI calculations. This limitation underscores the importance of combining DRI with complementary analytical techniques to achieve a more comprehensive understanding of damage mechanisms.

Similar to the previous study, Sanchez et al., (2015), highlights the DRI's ability to quantify ASR-related damage across a range of concrete strengths (25-45 MPa) and reactive aggregate types (fine jobe sand and coarse NM gravel). The findings demonstrated a near-linear correlation between DRI values and expansion levels (0.05–0.30%). This relationship was consistent across fine and coarse aggregates, with similar patterns of deterioration observed in 25 and 35 MPa concretes. However, 45 MPa concretes exhibited higher DRI values at 0.05% expansion, which stabilized at 0.12% before resuming an increasing trend.

Key observations included a notable increase in open cracks in aggregates and cement paste, with and without gel, as expansion progressed. These features strongly correlated with ASR-induced expansion, affirming the method's diagnostic potential. Closed cracks in aggregates showed more complex behavior, influenced by factors like aggregate weathering or processing. For reactive sand, closed cracks decreased with expansion up to 0.20%, as alkali hydroxides penetrated these channels, causing internal reactions and cracks extending into the cement paste. Beyond this point, closed cracks increased again, possibly due to ASR-induced pressure within the mortar.

Crack Density and Expansion

Crack density (CD) is defined as the sum of open cracks in the aggregate particles and cracks in the cement paste, with and without reaction products over the surface examined, normalized to counts/cm^2. The CD analysis revealed an increasing trend with specimen expansion, ranging from 0.4–1.2 cracks/cm² at 0.05% expansion to 2.2–3.5 cracks/cm² at ≥0.20% expansion. Notably, the alkali-carbonate reactive King + Lav mixture displayed higher CD values at lower expansions, stabilizing at approximately 3 cracks/cm² beyond 0.12% expansion (Figure 2-16). This suggests that while new cracks were limited, existing cracks expanded in width and length.

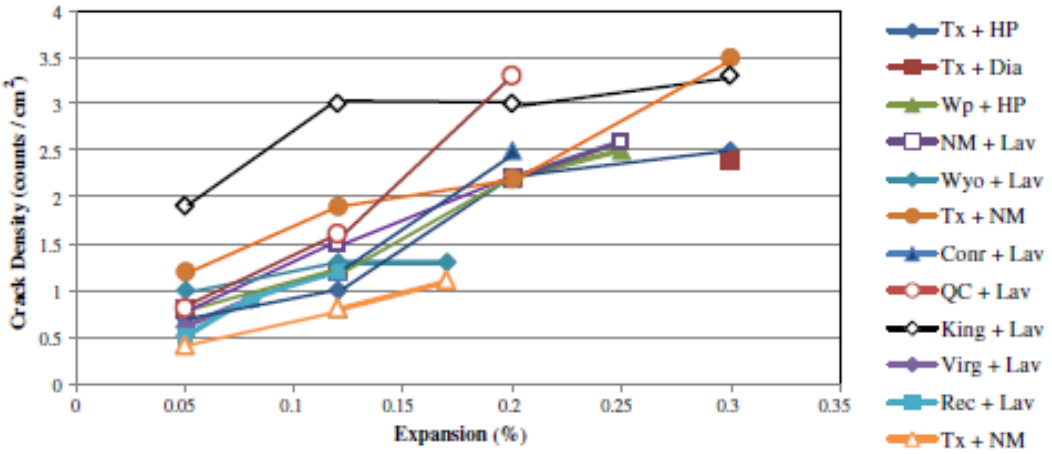

Figure 2-16 - Crack density as a function of expansion, adapted from (Sanchez et al., 2015)

2.5 Research Gap

One of the major challenges in evaluating the RC structures affected by deterioration mechanisms, such as corrosion, is the lack of a reliable framework to correlate microscopic damage features with the progression of distress, reduction in mechanical properties, and long-term durability. Existing assessment tools for corrosion-induced cracking predominantly focus on external or macroscopic evaluation, such as surface mapping, or non-destructive testing. While these methods are useful, they often lack the precision required to analyze microstructural damage comprehensively.

Microscopic evaluation, particularly using DRI, offers a systematic approach to quantify distress at a microstructural level, as demonstrated in its application for internal swelling reactions (ISR) like alkali-silica reaction (ASR), delayed ettringite formation (DEF), and freezing-thawing (FT) cycles. The DRI has proven effective in identifying specific damage signatures associated with ISR mechanisms, linking these features to expansion levels, mechanical property reduction, and durability losses. However, its application to assess damage induced by steel reinforcement corrosion remains largely unexplored.

Building on the proven capabilities of DRI in quantifying microscopic damage associated with internal swelling reactions, this study aims to critically evaluate whether the application of DRI is effective and sensitive for assessing damage mechanisms induced by steel reinforcement corrosion. By systematically analyzing deterioration features associated with corrosion-induced cracks, this study takes the initial steps for evaluating the applicability and reliability of the DRI protocol in capturing the progression of corrosion-related distress and integrating it into the existing DRI evaluation framework of deterioration induced by ISR mechanisms.

2.6. References

ACI Committee 224, 1R-07. 2007. "ACI Committee 224. (2007). ACI 224.1R-07: Causes, Evaluation, and Repair of Cracks in Concrete Structures."

Andrade, C., Gulikers, J., Polder, R., Cigna, R., Vennesland, O., Salta, M., & Raharinaivo, A. (2004). *RILEM TC 154-EMC: Electrochemical techniques for measuring metallic corrosion – Recommendations for test methods for on-site corrosion rate measurement of steel reinforcement in concrete by means of the polarization resistance method*. Materials and Structures, 37(273), 453–461. https://doi.org/10.1007/BF02481659

Aryanto, A., Revolis, M., Oribe, Y., & Yo, H. (2023). *Application of digital image correlation method in RC and FRC beams under bending test*. International Journal of GEOMATE, 24(101), 118–125. GEOMATE International Society. https://doi.org/10.21660/2023.101.g12275.

Barbosh, M., Dunphy, K., & Sadhu, A. (2022). *Acoustic emission-based damage localization using wavelet-assisted deep learning*. Journal of Infrastructure Preservation and Resilience, 3(1). Springer Nature. https://doi.org/10.1186/s43065-022-00051-8.

Berrocal, C. G., Fernandez, I., & Rempling, R. (2022). *The interplay between corrosion and cracks in reinforced concrete beams with non-uniform reinforcement corrosion*. Materials and Structures / Matériaux et Constructions, 55(4). Springer Science and Business Media B.V.

https://doi.org/10.1617/s11527-022-01956-2.

Bertolini, L. (Ed.). (2013). *Corrosion of steel in concrete: Prevention, diagnosis, repair*. Weinheim: Wiley-VCH.

Broomfield, J. P. (2007). *Corrosion of steel in concrete* (2nd ed.). New York, NY: Taylor & Francis.

Bungey, J. H., Millard, S. G., & Grantham, M. G. (2006). *Testing of concrete in structures* (4th ed.). London: CRC Press.

Dunbar, P. A., & Grattan-Bellew, P. E. (1995). *Results of damage rating evaluation of condition of concrete from a number of structures affected by AAR*. In Proceedings of the 12th International Conference on Alkali-Aggregate Reaction in Concrete (pp. 257–265). Ottawa, ON: Natural Resources Canada.

Erlin, B., & Stark, D. (1990). *Petrography applied to concrete and concrete aggregates*. In Petrography of Cementitious Materials, ASTM STP 1061, 63–84. ASTM International.

França de Mendonça Filho, F., Copuroglu, O., Schlangen, E., & Šavija, B. (2021). *Determination of loss of reinforcement due to corrosion through X-ray computer micro-tomography*. Materials, 14(4), 1–15. MDPI. https://doi.org/10.3390/ma14040893

Gonthina, M., Chamata, R., Duppalapudi, J., & Lute, V. (2023). *Deep CNN-based concrete cracks identification and quantification using image processing techniques*. Asian Journal of Civil Engineering, 24(3), 727–740. https://doi.org/10.1007/s42107-022-00526-9

Gonzalez, J. A., Felifi, S., Rodríguez, P., Ramírez, E., Alonso, C., & Andrade, C. (1996). *Some questions on the corrosion of steel in concrete – Part I: When, how and how much steel corrodes*. Materials and Structures, 29(1), 40–46. https://doi.org/10.1007/BF02485936

Grattan-Bellew, P. E., & Mitchell, L. D. (2006). *Quantitative petrographic analysis of concrete: The Damage Rating Index (DRI) method – A review*. In Proceedings of the 12th International Conference on Alkali-Aggregate Reaction (AAR) (pp. 321–334). Montréal: CANMET/ACI.

Guzmán, S., & Gálvez, J. C. (2017). *Modelling of concrete cover cracking due to non-uniform corrosion of reinforcing steel*. Construction and Building Materials, 155, 1063–1071. Elsevier. https://doi.org/10.1016/j.conbuildmat.2017.08.082

Guzmán-Torres, J. A., Domínguez-Mota, F. J., Martínez-Molina, W., Naser, M. Z., Tinoco-Guerrero, G., & Tinoco-Ruíz, J. G. (2023). *Damage detection on steel-reinforced concrete produced by corrosion via YOLOv3: A detailed guide*. Frontiers in Built Environment, 9. Frontiers Media S.A. https://doi.org/10.3389/fbuil.2023.1144606

Han, J., Miao, Z., Wang, J., Zhang, X., & Lv, Y. (2023). *Investigation of the corrosion-induced damage mechanism of steel fibers in ultra-high-performance steel fiber-reinforced concrete using X-ray computed tomography*. Construction and Building Materials, 368, 130429. Elsevier. https://doi.org/10.1016/j.conbuildmat.2023.130429

Jana, D. (2005). *Concrete petrography – past, present, and future*. In Proceedings of the 10th Euro seminar on Microscopy Applied to Building Materials, Paisley, Scotland.

Łaziński, P., Jasiński, M., Uściłowski, M., Piotrowski, D., & Ortyl, Ł. (2024). *GPR in damage identification of concrete elements – A case study of diagnostics in a prestressed bridge*. Preprints, 202411. https://doi.org/10.20944/preprints202411.0778.v1

Mak, M. W. T., Desnerck, P., & Lees, J. M. (2019). *Corrosion-induced cracking and bond strength in reinforced concrete*. Construction and Building Materials, 208, 228–241. Elsevier. https://doi.org/10.1016/j.conbuildmat.2019.02.151

Martin, R. P., Sanchez, L., Fournier, B., & Toutlemonde, F. (2017). *Evaluation of different techniques for the diagnosis and prognosis of internal swelling reaction (ISR) mechanisms in*

concrete. Construction and Building Materials, 156, 956–964. Elsevier. https://doi.org/10.1016/j.conbuildmat.2017.09.047

Neville, A. M. (1996). *Properties of Concrete* (4th ed.). New York: Wiley. ISBN: 9780470235270

Mehta, P. K., & Monteiro, P. J. M. (2001). *Concrete: Microstructure, properties, and materials* (3rd ed.). New York, NY: McGraw-Hill.

Kuntz, M., Bastien, J., & Perez, F. (2011). *Digital image correlation analysis of crack behavior in a reinforced concrete beam during a load test*. Canadian Journal of Civil Engineering, 33(11), 1411–1423. https://doi.org/10.1139/l06-081

Milovanović, B., & Pečur, I. B. (2016). *Review of active IR thermography for detection and characterization of defects in reinforced concrete*. Journal of Imaging, 2(2), 11. MDPI. https://doi.org/10.3390/jimaging2020011

Moccia, F., Fernández Ruiz, M., & Muttoni, A. (2021). *Spalling of concrete cover induced by reinforcement*. Engineering Structures, 237, 112188. Elsevier. https://doi.org/10.1016/j.engstruct.2021.112188

Mousa, M. A., Yussof, M. M., Hussein, T. S., Assi, L. N., & Ghahari, S. A. (2023). *A digital image correlation technique for laboratory structural tests and applications: A systematic literature review*. Sensors, 23(23), 9362. MDPI. https://doi.org/10.3390/s23239362

Nepal, J., & Chen, P. (2015). *Assessment of concrete damage and strength degradation caused by reinforcement corrosion*. IOP Conference Series: Materials Science and Engineering, 96, 012106. IOP Publishing. https://doi.org/10.1088/1757-899X/96/1/012106

Faris, N., Zayed, T., Abdelkader, E. M., & Fares, A. (2023). *Corrosion assessment using ground penetrating radar in reinforced concrete structures: Influential factors and analysis methods*. Automation in Construction, 156, 105130. https://doi.org/10.1016/j.autcon.2023.105130

Ohtsu, M., Shiotani, T., Shigeishi, M., Kamada, T., Yuyama, S., Watanabe, T., Suzuki, T., van Mier, J. G. M., Vogel, T., Grosse, C., Helmerich, R., Forde, M. C., Moczko, A., Breysse, D., Ivanovich, S. A., Sajna, A., Aggelis, D., & Lacidogna, G. (2010). *Recommendation of RILEM TC 212-ACD: Acoustic emission and related NDE techniques for crack detection and damage*

evaluation in concrete: Test method for damage qualification of reinforced concrete beams by acoustic emission. Materials and Structures / Matériaux et Constructions, 43(9), 1183–1186. Kluwer Academic Publishers. https://doi.org/10.1617/s11527-010-9639-z

Ongpeng, J. (2017). *Ultrasonic pulse velocity test of reinforced concrete with induced corrosion*. Engineering Journal, 7(2), 9–17. https://doi.org/10.11113/aej.v7.15490

Pan, B., Kemao, Q., Xie, H., & Asundi, A. (2009). *Two-dimensional digital image correlation for in-plane displacement and strain measurement: A review*. Measurement Science and Technology, 20(6), 062001. https://doi.org/10.1088/0957-0233/20/6/062001

Grattan-Bellew, P. E., & Danay, A. (1992). *Comparison of laboratory and field evaluation of AAR in large dams*. Canadian Electrical Association, in association with the Canadian National Committee of the International Commission on Large Dams.

Pfändler, P., Bircher, L., & Angst, U. (2022). *Inspecting the corrosion state of underground reinforced concrete structures*. Journal of Infrastructure Preservation and Resilience, 3(1), 12. Springer Nature. https://doi.org/10.1186/s43065-022-00064-3

Polder, R. B., & Peelen, W. H. A. (2014). *25 years of experience with cathodic protection of steel in concrete in the Netherlands*. In M. G. Alexander, H.-D. Beushausen, F. Dehn, & P. Moyo (Eds.), Durability of reinforced concrete: From composition to protection (pp. 69–75). Cham: Springer International Publishing. https://doi.org/10.1007/978-94-007-7854-2_6

Poole, A. B., & Sims, I. (2016). *Concrete petrography: A handbook of investigative techniques* (2nd ed.). London: CRC Press (Taylor & Francis Group).

Poursaee, A. (2016). *Corrosion of steel in concrete structures*. In A. Poursaee (Ed.), Corrosion of steel in concrete structures (pp. 19–33). Elsevier. https://doi.org/10.1016/B978-1-78242-381-2.00002-3

Rocha, J. H. A., & Póvoas, Y. V. (2019). *Detecção de corrosão em concreto armado com termografia infravermelha e ultrassom* [Detection of corrosion in reinforced concrete using infrared thermography and ultrasound]. Ambiente Construído, 19(3), 53–68. FapUNIFESP (SciELO). https://doi.org/10.1590/s1678-86212019000300324

Rodrigues, R., Gaboreau, S., Gance, J., Ignatiadis, I., & Betelu, S. (2021). *Reinforced concrete structures: A review of corrosion mechanisms and advances in electrical methods for corrosion monitoring*. Construction and Building Materials, 269, 121240. Elsevier. https://doi.org/10.1016/j.conbuildmat.2020.121240

Sansalone, M., & Streett, W. B. (1997). *Impact-echo: Non-destructive evaluation of concrete and masonry*. Michigan: Bullbrier Press.

Sanchez, L., Drimalas, T., & Fournier, B. (2020). *Assessing condition of concrete affected by internal swelling reactions (ISR) through the Damage Rating Index (DRI)*. Cement, 1–2, 100001. Elsevier. https://doi.org/10.1016/j.cement.2020.100001

Sanchez, L. F. M., Fournier, B., Jolin, M., Bedoya, M. A. B., Bastien, J., & Duchesne, J. (2016). *Use of Damage Rating Index to quantify alkali-silica reaction damage in concrete: Fine versus coarse aggregate*. ACI Materials Journal, 113(4), 395–407. American Concrete Institute. https://doi.org/10.14359/51688983

Sanchez, L. F. M., Fournier, B., Jolin, M., & Duchesne, J. (2015). *Reliable quantification of AAR damage through assessment of the Damage Rating Index (DRI)*. Cement and Concrete Research, 67, 74–92. Elsevier. https://doi.org/10.1016/j.cemconres.2014.08.002

Sanchez, L. F. M., Fournier, B., Jolin, M., Mitchell, D., & Bastien, J. (2017). *Overall assessment of alkali-aggregate reaction (AAR) in concretes presenting different strengths and incorporating a wide range of reactive aggregate types and natures*. Cement and Concrete Research, 93, 17–31. Elsevier. https://doi.org/10.1016/j.cemconres.2016.12.001

Sanchez, L. F. M. (2024). *Internal swelling reactions in concrete: Mechanisms and condition assessment*. CRC Press.

Shrimer, F. H. (2006). *Development of the Damage Rating Index method as a tool in the assessment of alkali-aggregate reaction in concrete: A critical review*. In Proceedings of the 12th International Conference on Alkali-Aggregate Reaction (AAR) (pp. 391–411). Montréal: CANMET/ACI.

Sims, I., Hunt, B., & Miglio, B. (1992). *Quantifying microscopical examinations of concrete for alkali-aggregate reactions (AAR) and other durability aspects*. In Proceedings of the 9th International Conference on Alkali-Aggregate Reaction in Concrete (ICAAR) (pp. 267–287). Detroit, MI.

Skarżyński, Ł., Kibort, K., & Małachowska, A. (2022). *3D X-ray micro-CT analysis of rebar corrosion in reinforced concrete subjected to a chloride-induced environment*. Molecules, 27(1), 192. MDPI. https://doi.org/10.3390/molecules27010192

Solla, M., Lorenzo, H., Rial, F. I., & Novo, A. (2012). *Ground-penetrating radar for the structural evaluation of masonry bridges: Results and interpretational tools*. Construction and Building Materials, 29, 458–465. https://doi.org/10.1016/j.conbuildmat.2011.10.001

Solla, M., Pérez-Gracia, V., & Fontul, S. (2024). *Corrosion assessment of reinforced concrete structures using ground-penetrating radar*. In Proceedings of the 9th International Conference on Civil, Structural and Transportation Engineering (ICCSTE 2024). Avestia Publishing. https://doi.org/10.11159/iccste24.XXX

Grzesiak, S., Basters, R., & de Sousa, C. (2023). *Application of computed tomography in structural engineering*. In Building for the Future: Durable, Sustainable, Resilient

Taheri-Shakib, J., & Al-Mayah, A. (2023). *4D evolutions of cracks, voids, and corrosion products in reinforced concrete materials*. Scientific Reports, 13(1), 2146. Nature Research. https://doi.org/10.1038/s41598-023-48058-9

Tešić, K., Baričević, A., & Serdar, M. (2021). *Non-destructive corrosion inspection of reinforced concrete using ground-penetrating radar: A review*. Materials, 14(4), 975. MDPI. https://doi.org/10.3390/ma14040975

Villeneuve, V., Fournier, B., Tremblay, S., Fecteau, P. L., & Sanchez, L. (2011). *Description des indices pétrographiques pour analyse pétrographique semi-quantitative du béton selon la méthode du Damage Rating Index*. Laval, QC: Université Laval.

Villeneuve, V., Fournier, B., & Duchesne, J. (2008). *Determination of the damage in concrete affected by ASR – The Damage Rating Index (DRI)*. Québec, QC: Université Laval.

Yadeta, K. F., Siriwardane, S. C., & Mohammed, T. A. (2023). *Service life prediction of reinforced concrete structures subjected to corrosion: A comparative study*. International Journal of Structural Integrity, 14(3), 480–497. Emerald Publishing. https://doi.org/10.1108/IJSI-12-2022-0149

Yu, X. R., Yan, Z. T., & Li, J. H. (2024). *Comprehensive study on corrosion-induced structural deterioration of steel bars in reinforced concrete beams*. Journal of Constructional Steel Research, 214, 108504. Elsevier. https://doi.org/10.1016/j.jcsr.2024.108504

Zahedi, A., Sanchez, L. F. M., & Noël, M. (2022). Effect of confinement on AAR-induced expansion and damage. In *Proceedings of the 16th International Conference on Alkali-Aggregate Reaction in Concrete (ICAAR)* (pp. 757–767).

Zahedi, A., Trottier, C., Sanchez, L. F. M., & Noël, M. (2021). *Microscopic assessment of ASR-affected concrete under confinement conditions*. Cement and Concrete Research, 145, 106456. Elsevier. https://doi.org/10.1016/j.cemconres.2021.106456

Zhang, Y., & Su, R. K. L. (2020). *Experimental investigation of the process of corrosion-caused cover cracking*. Construction and Building Materials, 253, 119166. Elsevier. https://doi.org/10.1016/j.conbuildmat.2020.119166

Zhou, Y., Gencturk, B., Willam, K., & Attar, A. (2015). *Carbonation-induced and chloride-induced corrosion in reinforced concrete structures*. Journal of Materials in Civil Engineering, 27(9), 04014252. American Society of Civil Engineers (ASCE). https://doi.org/10.1061/(ASCE)MT.1943-5533.0001209

3 Research Methodology

3.1 Overview

Chapter 3 outlines the experimental methodology employed to investigate corrosion-induced cracking in the RC structures.

The chapter begins with a description of the test specimens, which include various geometries, reinforcement types, and water-to-cement ratios, designed to simulate diverse structural and environmental conditions affecting corrosion. Details are provided on the selection of materials, including the use of non-reactive aggregates and specific mixture proportions aimed at controlling workability, strength, and permeability of the concrete.

The casting and curing processes are then described, emphasizing the controlled environment used to ensure consistent hydration and strength development before exposure to accelerated corrosion. Following curing, the specimens were subjected to an accelerated corrosion regime using a constant current density to achieve a targeted mass loss, replicating the corrosion-induced deterioration in real structures.

This study did not include a post-corrosion forensic analysis of the reinforcing bars; specially, rebar morphology was not characterized, and gravimetric mass loss was not measured, as the scope focused on concrete-side damage quantification.

Finally, the DRI protocol is introduced as a tool for assessing distress features and quantifying the extent of damage across different specimen materials and detailing configurations.

3.2 Test Specimens

The test specimens used in this study were designed to evaluate the effect of corrosion-induced cracking in the RC. A total of 24 cylindrical specimens with three geometries (Φ 75 mm × 150 mm, Φ 100 mm × 200 mm, and Φ 150 mm × 300 mm), as illustrated in Figure 3-1, and two water-to-cement ratios (0.4 and 0.54) were fabricated in the laboratory. The specimens were singly reinforced at their centers with either a 10M or 20M reinforcing steel bar, with a yield strength of 400 MPa (CSA G30.18:21, 2021). The reinforcing steel bars extended 20 mm above the top surface

of the concrete cylinders. The geometry and reinforcing steel bars were selected to achieve different concrete cover-to-rebar diameter ratios (C/D), ranging from 1.42 to 6.14 (Table 3-1).

While a total of 24 specimens were fabricated and tested, 2 identical samples with the same C/D and W/C were fabricated for reproducibility of results.

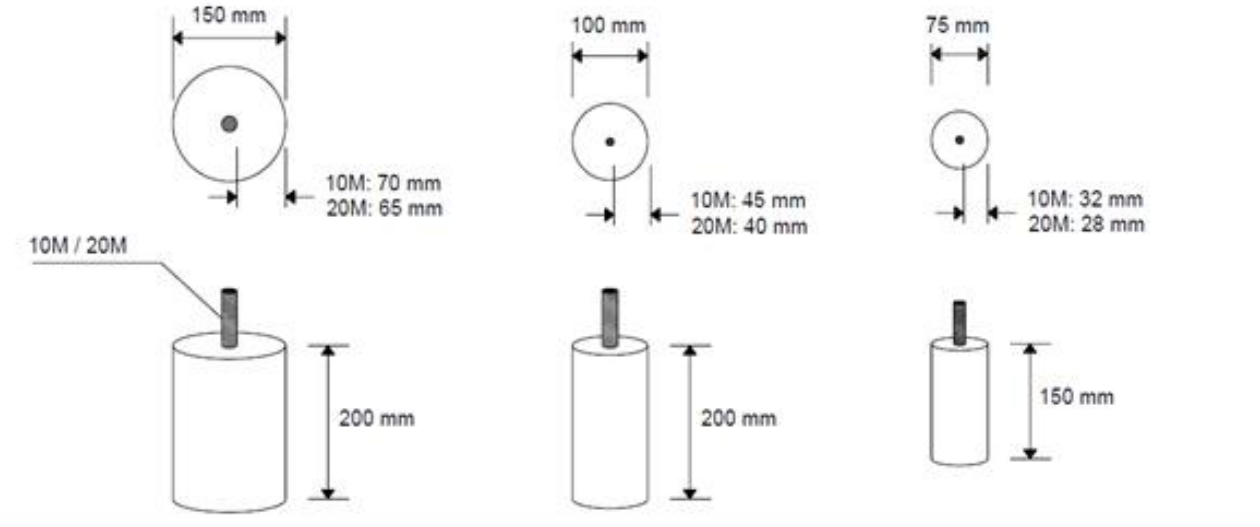

Figure 3-1- Concrete cylinder dimensions

Table 3-1 - Details of test specimens with geometries, reinforcement, and corrosion parameters

	Sample ID – Qty: (2 each) (mm)	C/D Ratio	W/C Ratio	Steel Nominal Diameter (mm)	Steel Length (mm)	Steel Mass per Unit Length (kg/m)	Mass for specified Length (g)	I corr – electrical current (μA)	Targeted Mass Loss (g)[1]	Days needed to be corroded
1	Φ 75 × 150	1.42	0.40	19.5	170	2.355	400.4	15622	20.01	51
2	Φ 100 × 200	2.06	0.40	19.5	220	2.355	518.1	20216	25.91	51
3	Φ 75 × 150	2.82	0.40	11.3	170	0.785	133.4	9052.5	6.67	29
4	Φ 150 × 300	3.35	0.40	19.5	320	2.355	753.6	29405	37.68	51
5	Φ 100 × 200	3.92	0.40	11.3	220	0.785	172.7	11715	8.635	29
6	Φ 150 × 300	6.14	0.40	11.3	320	0.785	251.2	17040	12.56	29
7	Φ 75 × 150	1.42	0.54	19.5	170	2.355	400.4	15622	20.01	51
8	Φ 100 × 200	2.06	0.54	19.5	220	2.355	518.1	20216	25.91	51
9	Φ 75 × 150	2.82	0.54	11.3	170	0.785	133.4	9052.5	6.67	29
10	Φ 150 × 300	3.35	0.54	19.5	320	2.355	753.6	29405	37.68	51
11	Φ 100 × 200	3.92	0.54	11.3	220	0.785	172.7	11715	8.635	29
12	Φ 150 × 300	6.14	0.54	11.3	320	0.785	251.2	17040	12.56	29

[1]Targeted mass loss is theoretically calculated using Faraday's law; no gravimetric mass testing was performed.

3.3 Materials and Mixture Proportions

To investigate the influence of concrete microstructure on corrosion-induced cracking, two water-to-cement (W/C) ratios, 0.4 and 0.54, were selected. These ratios were chosen to explore the impact of concrete, microstructure and strength on cracking initiation, propagation and patterns.

The concrete mixtures were proportioned to achieve the specified W/C ratios, and included General Use (GU) cement, non-reactive limestone coarse aggregate with a nominal diameter of 19 mm, and natural non-reactive sand as the fine aggregate. The limestone coarse aggregate was

selected because it is non-reactive, minimizing the risk of alkali-silica reaction, and because limestone is among the most widely used aggregates in Ontario, thereby ensuring that the test results reflect conditions representative of common local practice. The mixing water contained 5% NaCl by weight of cement to induce corrosion. The mixture proportions are tabulated in Table 3-2.

Table 3-2 - Material type, mix-design proportions and properties

W/C ratio 0.4					
Material	Proportion (kg/m^3)	Type	Specific gravity	Absorption (%)	Fineness Modulus
Cement	420	GU	---	---	---
Coarse aggregate	1054	Non-reactive Limestone 19mm Tomlinson	2.78	0.42	---
Fine aggregate	838	Non-reactive natural sand	2.67	1.25	2.85
Water	163	---	---	---	---
NaCl	35	---	---	---	---
W/C ratio 0.54					
Cement	343	GU	---	---	---
Coarse aggregate	1054	Non-reactive Limestone 19mm Tomlinson	2.78	0.42	---
Fine aggregate	856	Non-reactive natural sand	2.67	1.25	2.85
Water	180	---	---	---	
NaCl	28	---	---	---	

3.4 Casting and Curing

The preparation of the concrete cylinders involved placing the reinforcing steel bars centrally within the empty moulds, as shown in Figure 3-2a. Once the reinforcements were properly positioned, the concrete mixtures were cast into the molds and compacted to remove air voids, as shown in Figure 3-2b. After casting, the cylinders were left to set for 24 hours before demolding, during which hydration conditions were maintained to prevent evaporation.

(a) **(b)**

Figure 3-2 - Concrete cylinders with centrally reinforcing steel bars prior to casting & (b) Concrete cylinders immediately after casting

All cylinders were demolded 24 hours after casting and subsequently transferred to a curing environment, where they were placed in a moist curing bin at a constant temperature of 23 ± 2ºC (73 ± 4ºF) for 28 days. This process ensured that the concrete specimens achieved adequate strength prior to exposure to the accelerated corrosion regime. Throughout the curing process, precautions were taken to prevent moisture loss. Figure 3-3 shows the fully cured concrete samples after the 28-day curing period, before being subjected to an accelerated corrosion regime.

Figure 3-3 - Concrete specimens after 28 days of curing, ready for accelerated corrosion test

3.5 Compressive Strength

For the compressive strength tests, non-reinforced concrete cylinders were cast alongside the reinforced specimens. These non-reinforced cylinders were used to assess the concrete's mechanical properties at 7, 14, and 28 days after casting, in accordance with “CSA A23.1/A23.2” (2019), as illustrated in Figure 3-4. Due to limited availability of materials, the 14-day compressive strength test for the 0.4 W/C ratio was not conducted. However, two additional non-reinforced cylinders were cast for the 7-day and 28-day tests for each mix.

Figure 3-4 - Concrete specimens during compressive strength test

The results of the compressive strength tests at 7 and 28 days are summarized in Figure 3-5.

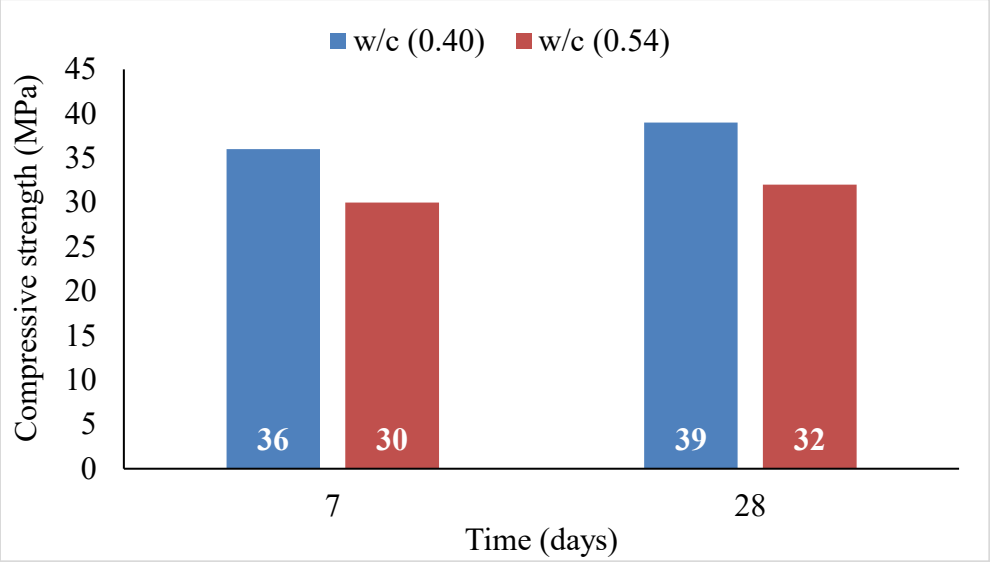

Figure 3-5 - Compressive strength test results for concrete cylinders

3.6 Accelerated Corrosion Regime

The experimental setup involved subjecting the RC cylinders to an accelerated corrosion regime to induce corrosion in the reinforcing bars.

Following 28 days of curing, the specimens were wrapped in natural burlap fabric (Figure 3-6a), to maintain moisture levels, and then further wrapped with stainless steel wire mesh, (Figure 3-6b), which served as the cathode in the corrosion process. Figure 3-6c illustrates the final wrapped sample.

Each concrete specimen was cast with embedded steel reinforcement extending 20 mm beyond the concrete surface at the top end to allow for electrical connectivity. These extended steel ends enabled secure attachment to the positive terminal of a direct current (DC) power supply using clamp connections (Figure 3-8). The specimens were electrically connected in parallel, as illustrated in Figure 3-9, ensuring that each sample within a given group experienced uniform current flow. Groups were assembled based on shared geometry and compositional characteristics to maintain consistent electrical resistivity and corrosion conditions across all samples within the group.

(a) **(b)** **(c)**

Figure 3-6 - (a)Natural burlap fabric used for moisture retention in accelerated corrosion regime (b) Stainless steel wire mesh used as cathode in the accelerated corrosion setup (c) Burlap-wrapped reinforced concrete cylinders with stainless steel mesh for corrosion testing

The applied electrical current I_{corr} was adjusted to achieve a constant current density of 150 µA/cm² based on both practical and experimental considerations. Previous studies have shown current densities ranging from 10 µA/cm² to 100 µA/cm², simulate the maximum corrosion rates observed in carbonated or chloride-contaminated concrete in the field (Andrade et al. 1993). However, due to time constraints in this study, a higher current density of 150 µA/cm² was selected to induce corrosion within a shortened experimental timeline. The corresponding electrical current I_{corr} was calculated from:

$$i_{corr} = \frac{I_{corr}}{\pi d_b L} \qquad \text{(Equation 3.1)}$$

where,

i_{corr} = current density (A/m^2)
I_{corr} = electrical current (A)

d_b = reinforcing steel diameter (e.g., d_b = 11.3 ×10^{-3} m for 10M)

L = reinforcing steel length (m)

The accelerated corrosion regime was carried out for a period of time t to achieve a target steel mass loss of 5%. The duration of the test was calculated from Faraday's law:

$$m_s = \frac{M}{zF} \cdot I_{corr} \cdot t \qquad \text{(Equation 3.2)}$$

where,

m_s = mass loss (g),

M = metal molar mass (55.85 g/mol for iron)

z = valence of the ion formed because of iron oxidation (i.e., z = 2 for $Fe \rightarrow Fe^{2+}+2e^{-}$)

F = Faraday's constant (F = 96,485 C/mol)

I_{corr} = corrosion current (A)

t = time elapsed since the beginning of the accelerated corrosion regime (s)

Equation 3.2 assumes that the applied electrical current I_{corr} is 100% efficient in the corrosion process. Table 3-1 lists the time each specimen underwent accelerated corrosion to achieve the theoretical 5% target mass loss.

The target mass loss values in Table 3-1 were calculated from Faraday's law, assuming 100% current efficiency and were not validated by gravimetric measurements. After the accelerated regime, no metallographic or morphological examination of the rebars was performed. Consequently, the corrosion level referenced throughout this work should be interpreted as a theoretical target used to standardize exposure, while the analysis concentrates on the resulting concrete microstructural damage.

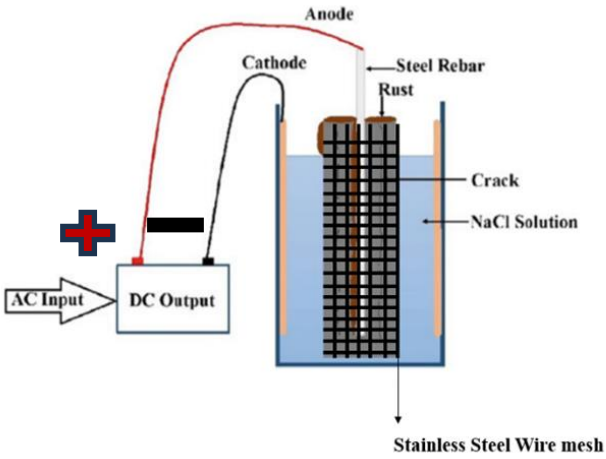

Figure 3-7 - Schematic of the impressed current setup, adapted from Bhattacharjee (2020)

(a) (b) (c)

Figure 3-8 - (a) Clamp connections to 10M and 20M rebar protrusions for accelerated corrosion (b) Specimen connected to power source; (c) Close-up of corroded rebar connection

Figure 3-9 - Accelerated corrosion setup: concrete specimens in NaCl solution connected to the power supply

3.7 Damage Rating Index: The Method

The DRI methodology (Sanchez et al., 2015) was employed to assess its reliability and sensitivity in evaluating the degree of damage caused by corrosion in the RC specimens. This approach enables a detailed correlation between observed microscopic damage and design-related parameters, such as water-to-cement (W/C) ratio and concrete-cover-to-rebar-diameter (C/D) ratio, offering valuable insights into the implications of corrosion-induced damage.

3.7.1 Samples Preparation and Polishing

The preparation of concrete samples is critical to the accuracy and reliability of DRI measurements. In this study, cylindrical specimens were cut longitudinally using a diamond saw and polished to achieve a highly reflective surface suitable for petrographic examination.

The grinding and polishing process was carried out using a series of polishing surfaces with varying abrasiveness to gradually refine the concrete surface. Each polishing level was applied for approximately 10 minutes to ensure a consistent finish across all specimens. After each stage, the specimens were cleaned using a soft brush and compressed air to remove any remaining slurry, loose abrasives, and dislodged particles from the surface of the aggregate and cement paste.

Surface quality was evaluated by reflecting sunlight- onto the prepared surface to identify areas lacking reflectivity, which appear dull or white. Any deep scratches or residual marks from earlier

steps were removed before advancing. The marks progressively diminished as the surface became adequately polished (Figure 3-10).

(a) (b)

Figure 3-10 - (a) unpolished & (b) polished concrete surface

Once a smooth, reflective surface suitable for analysis was achieved, a 1×1 cm 3D-printed grid used (Figure 3-11).

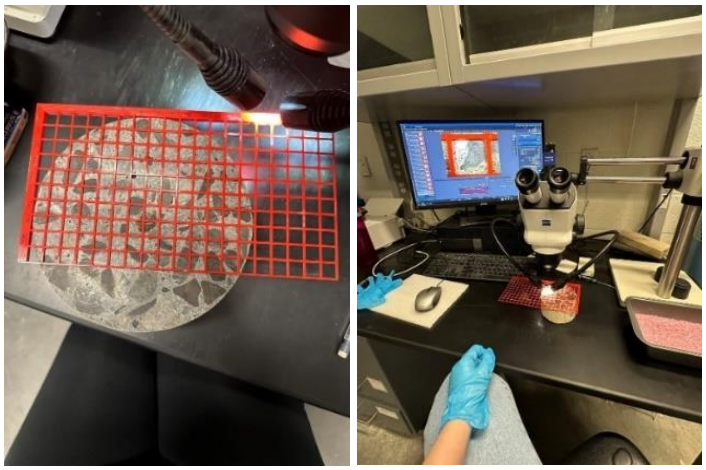

(a) (b)

Figure 3-11 - (a) One cm^2 mesh grid on the polished sample (b) microscopic analysis using the DRI protocol

3.8 References

Alonso, C., Andrade, C., & Diez, J. M. (1998). *Factors controlling cracking of concrete affected by reinforcement corrosion*. Materials and Structures / Matériaux et Constructions, 31(211), 435–441. https://doi.org/10.1007/BF02480474

Bhattacharjee, B., Shukla, S. K., Raman, S. N., & Bhattacharjee, J. (Eds.). (2021). *Advances in geotechnics and structural engineering: Select proceedings of TRACE 2020* (Lecture Notes in Civil Engineering, Vol. 143). Singapore: Springer. https://doi.org/10.1007/978-981-33-6969-6

Canada Standards Association (CSA Group). (2019). *CSA A23.1:19 / CSA A23.2:19 – Concrete materials and methods of concrete construction / Test methods and standard practices for concrete*. Toronto, ON: CSA Group.

Canada Standards Association (CSA Group). (2021). *CSA G30.18:21 – Carbon steel bars for concrete reinforcement*. Toronto, ON: CSA Group.

Sanchez, L. F. M., Drimalas, T., & Fournier, B. (2020). *Assessing condition of concrete affected by internal swelling reactions (ISR) through the Damage Rating Index (DRI)*. Cement, 1–2, 100001. Elsevier. https://doi.org/10.1016/j.cement.2020.100001

Sanchez, L. F. M., Fournier, B., Jolin, M., Bedoya, M. A. B., Bastien, J., & Duchesne, J. (2016). *Use of Damage Rating Index to quantify alkali-silica reaction damage in concrete: Fine versus coarse aggregate*. ACI Materials Journal, 113(4), 395–407. American Concrete Institute. https://doi.org/10.14359/51688983

Sanchez, L. F. M., Fournier, B., Jolin, M., & Duchesne, J. (2015). *Reliable quantification of AAR damage through assessment of the Damage Rating Index (DRI)*. Cement and Concrete Research, 67, 74–92. Elsevier. https://doi.org/10.1016/j.cemconres.2014.08.002

4 Assessment of the Damage Rating Index (DRI) as a Tool for Quantifying Corrosion-Induced Damage in Reinforced Concrete

Abstract

The Damage Rating Index (DRI), a microscopic and semi-quantitative petrographic tool, is a method increasingly recognized for its ability to assess the extent of damage in concrete affected by various deterioration mechanisms. This study evaluates the reliability and applicability of the DRI to quantify damage in reinforced concrete specimens subjected to reinforcement corrosion-induced cracking. Reinforced concrete cylinders with varying water-to-cement (W/C) ratios and concrete cover-to-rebar diameter (C/D) ratios were analyzed to assess the DRI's sensitivity in capturing the extent of damage at a target steel mass loss of 5%. The results demonstrate that the DRI effectively captures microstructural damage, particularly the development of cracks in the cement paste with and without products, which are key indicators of corrosion development. A classification of corrosion-induced damage based on DRI is then proposed, reinforcing its potential as a diagnostic tool for assessing reinforced concrete deterioration.

Keywords: corrosion-induced damage; corrosion-induced crack analysis; Damage Rating Index; corrosion-affected reinforced concrete; durability assessment; deterioration features.

4.1 Introduction

Reinforced concrete (RC) is a widely used construction material known for its mechanical properties and durability. Despite its versatility, the RC performance can be compromised by corrosion of steel reinforcement. Corrosion is an electrochemical process that generates expansive products, leading to cracking, spalling, and delamination of the concrete cover (Bertolini, 2013; Hwang & Yong Ann, 2023). This deterioration reduces the structural capacity, affecting the service life of the RC elements and posing risks to critical infrastructure (Tian et al., 2023). Although the half-cell potential and linear polarization techniques are often used in the laboratory and in the field to assess corrosion potential and rate (Sadowski, 2013), respectively, advanced tools, particularly microscopic techniques, are still required to quantify the extent and progression of corrosion-induced damage in the RC over time.

In this context, the Damage Rating Index (DRI) has emerged in recent years as a reliable microscopic tool to assess the deterioration of concrete due to internal swelling mechanisms. The DRI was originally developed by Grattan-Bellew and colleagues (Grattan-Bellew et al., 2006), to assess concrete affected by alkali-silica reaction (ASR). The method involves counting and weighting specific features of damage observed in polished concrete sections, enabling the estimation of the mechanism affecting the concrete (i.e., cause) and the severity (i.e., extent) of the induced deterioration (Sanchez et al., 2017). Since its development, the DRI has been effectively used (Sanchez et al., 2015), to assess damage caused by internal swelling reactions (ISRs) such as ASR, delayed ettringite formation (DEF), and freeze-thaw (FT) cycles (Sanchez et al., 2018). However, the DRI has never been utilized to appraise corrosion-induced deterioration. This work aims to evaluate the applicability of the current DRI protocol in assessing corrosion-induced cracking, focusing on understanding its effectiveness as a diagnostic test protocol.

4.1.1 Corrosion-Induced Cracking

The RC structures face various durability challenges, with corrosion of embedded steel reinforcement being one of the most critical mechanisms of deterioration (Bertolini, 2013). Corrosion typically initiates at the steel-concrete interface when the protective passive layer is disrupted, often due to carbonation or chloride ingress (Andrade et al., 1993; Broomfield, 2007). This disruption leads to the formation of expansive non-adherent corrosion products, which occupy two to six times the volume of the original steel (Broomfield 2007). The resulting volumetric expansion generates internal stresses that eventually exceed the tensile strength of the surrounding concrete, causing cracks originating at the steel-concrete interface (Alonso et al., 1998). These cracks propagate mainly through the cement paste, progressively weakening the bond between the steel and the concrete (Ahmad, 2003; Broomfield, 2007).

Corrosion-induced cracking is a critical concern for the long-term performance and service life of the RC structures, as it significantly compromises their structural integrity (Huy Tang Bui et al., 2024). Over time, the widening of these cracks leads to concrete cover spalling, further exposing steel reinforcement to environmental conditions. This exposure accelerates the corrosion process, intensifying structural deterioration (Broomfield, 2007). The crack features (i.e., area, density, and the presence of reaction products) associated with corrosion are influenced by factors including

the water-to-cement (W/C) ratio, concrete cover-to-rebar diameter (C/D) ratio, and environmental exposure conditions (Berrocal et al., 2022).

Despite advancements in tools for assessing corrosion-induced damage in concrete, most methods rely on macroscopic evaluations of externally visible signs of deterioration. This limits their capacity to capture detailed information about the damage process, particularly the characteristics of cracking at the early stages of deterioration. Moreover, while some microscopic analysis techniques have been found suitable for assessing damage in concrete such as the DRI, they have never been used to evaluate corrosion-induced deterioration (Sanchez et al., 2016).

4.1.2 The Damage Rating Index (DRI)

DRI is a microscopic technique conducted through a stereomicroscope with a magnification of 15 - 16x; it involves systematically identifying and counting microscopic damage features within 1 cm^2 (0.155 in^2) grids marked on the surface of polished concrete sections, as illustrated in Figure 4-1 (Villeneuve et al., 2012). In the DRI protocol, the counts of each type of microscopic distress feature are multiplied by weighting factors (Table 4-1), whose purpose is to balance the relative importance toward the overall damage of the affected material. Since its inception, the DRI has been primarily used to evaluate internal swelling reactions, particularly ASR.

Grattan-Bellew & Danay proposed the DRI to initially evaluate ASR-induced development. Such a technique has emerged from the difficulty of conventional petrographic analysis in capturing the extent of deterioration of affected concrete. The initial DRI protocol encompassed assessing petrographic ASR-related features, such as cracks in the aggregates and cement paste, with and without gel, along with pores filled by gel and reaction products. Weighting factors were then arbitrarily proposed to balance the importance of each petrographic feature towards ASR advancement (Dunbar, 1995; Grattan-Bellew et al., 1992; Sanchez et al., 2015).

Since initially proposed in 1992, the DRI has been modified/improved by several researchers, changing the size of individual evaluation grids, modifying/adding weighting factors to better represent ASR-induced damage along with reducing the variability among operators (Clemeña et al., 2000; Grattan-Bellew & Danay, 1992; Powers & Shrimer, 2007; Rivard et al., 2000; Smaoui et al., 2004).

The most recent version of DRI was proposed by Villeneuve and Fournier in 2010 to distinguish petrographic features from microscopic distress features while adjusting the weighting factors to better capture induced expansion and damage. These adjustments were validated in an intra-laboratory program, obtaining a promising and acceptable 20% variability among operators (Villeneuve, 2011; Villeneuve et al., 2012). Later, Sanchez et al. (2015) have adopted the method to assess ASR induced damage originating in fine-reactive aggregates, adjusting the size of cracks counted down to 1mm, along with validation of the method to assess distress caused by other mechanisms, such as delayed ettringite formation (DEF) and freeze and thaw (FT), single or combined with ASR. Furthermore, Sanchez (2015, 2024) have developed an extended version of the DRI, which helps understand the deterioration process on the microscopic scale. The developments above showed the important connection between the DRI outcomes and the mechanical properties reductions of deteriorated concrete (Sanchez et al., 2015, 2016, 2017, 2018).

The distress features included in the current DRI protocol and the respective weighting factors are listed in Table 4-1. The closed crack in the aggregates (CCA) is generally a feature caused by weathering and/or aggregates manufacturing. Since it is a pre-existing distress feature of the aggregate, not necessarily related to the damage mechanism occurring in the concrete, it stands with a low weighting factor (i.e., 0.25). Open cracks in the aggregate particles without or with reaction products (OCA and OCA-RP, respectively) are frequently observed damage features associated with mechanisms triggered by the aggregates; thus, an important weighting factor of 2 is given to such distress features. A higher weighting factor of 3 is attributed to cracks in the cement paste with or without reaction products (CCP-RP and CCP, respectively), since those cracks reflect a more severely damaged concrete, possibly being generated by cement paste mechanisms, advanced stages in mechanisms triggered by the aggregates, or loading. Finally, the two other remaining distress features (i.e., disaggregated aggregate particles DAP, with the weighting factor of 2, and aggregate debonding CAD with the weighting factor of 3, represent distress features less often observed, but that may happen due to damage mechanisms that are either generated in the aggregates or cement paste.

Table 4-1 - (a) DRI distress features and weighting factors, adopted from Villeneuve et al. (2012)

Damage features		Weighing factor
Aggregate	Closed crack (CCA)	0.25
	Opened crack (OCA)	2
	Opened crack with reaction product (OCA_RP)	2
Coarse aggregate debonded (CAD)		3
Disaggregate/corroded aggregate particle (DAP)		2
Crack in the cement paste (CCP)		3
Crack in the cement with reaction product (CCP_RP)		3

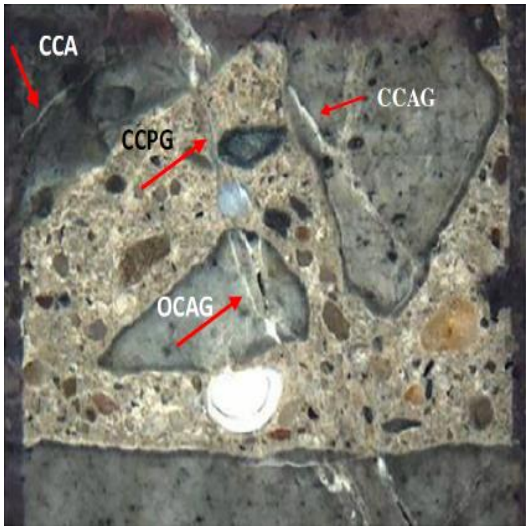

Figure 4-1- (b) Features of deterioration of DRI in a 1 cm2 grid (Sanchez et al., 2018)

For the optimal use of the DRI, it is generally recommended that a 200 cm² polished concrete section per structural member of interest be analyzed. In cases involving mass concrete with larger aggregate particles, larger sections may be required to capture the full range of petrographic features and ensure reliable assessments; however, for consistency purposes, the final DRI number is standardized to a 100 cm² (15.5 in²) area (Shrimer 2006).

Finally, to evaluate the efficiency of the DRI in appraising corrosion-induced damage, (i.e., including weighting factors), the following questions should be addressed:

- How effective and reliable is the current version of the DRI in evaluating corrosion-induced damage in concrete?
- How sensitive is the current version of the DRI in identifying the extent of corrosion-induced damage in concrete if key parameters influencing the deterioration process are changed, such ass the water-to-cement and concrete- cover-to-rebar diameter ratios?

4.2 Research Significance

As previously indicated, the DRI has been shown to be a reliable microscopic technique for diagnosing (i.e., cause and extent) concrete damage due to internal swelling mechanisms. Given that corrosion-induced damage results in concrete cracking originating at the steel/concrete interface and propagating toward the external concrete surface or nearby reinforcing bars, there is a potential of using the DRI for assessing corrosion-induced deterioration. This work examines the potential for DRI to quantify corrosion-induced damage in concrete. The RC cylinders were manufactured, demolded after 24 hours, and placed in a moist-curing chamber maintained at 23 ± 2°C (73 ± 4°F) for 28 days to ensure adequate hydration and strength development. Following the curing period, the specimens were exposed to an accelerated corrosion regime, with an applied galvanostatic current density of 150 μA/cm². Based on Faraday's Law calculations, specimens remained under these conditions to reach a target steel mass loss of 5% before being prepared for DRI analysis.

4.3 Materials and Methods

4.3.1 Materials and Mixture Proportions

The microscopic damage evaluations were performed on the RC cylinders with varying geometries and reinforcement configurations to evaluate corrosion-induced cracking. A total of 24 cylindrical specimens were fabricated, featuring three sizes (i.e., Φ 75 mm × 150 mm, Φ 100 mm × 200 mm, and Φ 150 mm × 300 mm), and two water-to-cement (W/C) ratios (i.e., 0.4 and 0.54), with two identical specimens for each geometric configuration and W/C. The W/C ratios of 0.4 and 0.54 were selected to examine the influence of mechanical properties on corrosion-induced damage. The W/C ratio of 0.4 was selected based on CSA A23.1/A23.2 (2019) as a standard for durable concrete, while the 0.54 ratio represents a lower-quality material to examine its impact on corrosion-induced damage. Each specimen was centrally reinforced with either a 10M or 20M steel bar, with a yield strength of 400 MPa ("CSA G30.18:21," 2021). The selected sizes allowed for the investigation of concrete cover-to-rebar diameter (C/D) ratios, ranging from 1.42 to 6.14, as detailed in Table 4-2. The reinforcing steel bars extended 20 mm (0.79 in) beyond the concrete surface to accommodate the clamp connections required to accelerate the corrosion process.

The concrete mixtures included General Use (GU) Portland cement, nonreactive limestone coarse aggregate (nominal size of 19 mm), and natural nonreactive sand as fine aggregate (Table 4-3).

The mixing water contained 5% NaCl by weight of cement (Andrade et al., 1993; Liu & Weyers, 1998) to induce reinforcing steel depassivation and initiate the corrosion process. The mixture proportions are summarized in Table 4-4.

Table 4-2 - Cylinder geometries and C/D ratios

Cylinder geometry (mm)	Bar size	Steel diameter (mm)	C/D ratio
Φ 75 × 150	10	11.3	2.82
Φ 75 × 150	20	19.5	1.42
Φ 100 × 200	10	11.3	3.92
Φ 100 × 200	20	19.5	2.06
Φ 150 × 300	10	11.3	6.14
Φ 150 × 300	20	19.5	3.35

Table 4-3 - Characteristics of materials

Material	Type	Specific gravity	Absorption (%)	Fineness modulus
Cement	GU	-	-	-
Coarse aggregate	Non-reactive Limestone 19mm Tomlinson	2.78	0.42	-
Sand	Non-reactive natural sand	2.67	1.25	2.85

Table 4-4 - Concrete mix proportions

Material	Materials [kg/m^3]	
	Water-Cement Ratio 0.40	**Water-Cement Ratio 0.54**
Cement	420	343
Sand	838	856
Coarse aggregate	1054	1054
Water	163	180

Compressive strength tests were conducted on plain companion concrete cylinders cast alongside the reinforced specimens. The tests followed CSA A23.1/A23.2 (2019) and were performed at 7 and 28 days after casting. The results of the compressive strength tests at 7 and 28 days are summarized in Table 4-5.

Table 4-5 - Compressive strength test results for concrete cylinders

Time (days)	W/C = 0.40 (MPa)	W/C = 0.54 (MPa)
7	36	30
28	39	32

4.3.2. Curing and Accelerated Corrosion of Test Specimens

After casting, all concrete cylinders were demolded after 24 hours and transferred to a moist-curing chamber maintained at 23 ± 2°C (73 ± 4°F). This curing regime was sustained for 28 days to ensure adequate hydration and development of mechanical properties. The curing process was carefully controlled to minimize moisture loss and prevent early cracking, ensuring the specimens achieved sufficient strength prior to applying the galvanostatic accelerated corrosion regime.

Previous studies have used current densities ranging from 10 to 100 μA/cm² to simulate typical corrosion rates observed in carbonated or chloride-contaminated concrete (Gonzalez et al., 1996).

However, to expedite the deterioration process within the study's timeframe, a higher current density of 150 μA/cm² was applied. To simulate chloride-induced corrosion, two-thirds of the specimens were partially immersed in a 5% NaCl solution, ensuring sufficient chloride exposure to depassivate the reinforcing steel and sustain active corrosion. The specimens were designed with reinforcing bars extending 20 mm beyond the concrete surface at the top (Figure 4-2a), allowing for secure clamp connections to the DC power supply. The specimens were connected in parallel (Figure 4-2b) to ensure uniform current distribution within each test group. Each group consisted of concrete cylinders with identical geometries and W/C ratios, thereby maintaining similar microstructural properties and electrical resistivity. This grouping approach ensured that all specimens within a parallel circuit experienced comparable corrosion conditions, allowing for consistent evaluation of corrosion-induced damage across similar material configurations.

The duration required to achieve a 5% steel mass loss target was determined using Faraday's law, considering the applied current density, reinforcement length, and bar size. Once the specimens reached this target level of corrosion, they were extracted from the setup and prepared for Damage Rating Index (DRI) analysis.

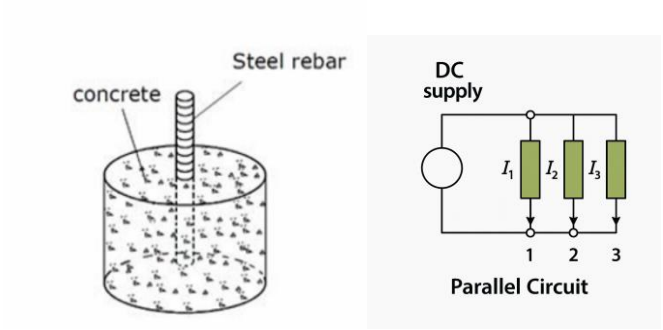

(a) **(b)**

Figure 4-2 - (a) Reinforced concrete cylinder; (b) Parallel circuit

4.3.2 Methods for Assessment and Analysis

The DRI was conducted on all concrete specimens, presenting distinct W/C and C/D ratios. Samples used for DRI analysis were obtained by cutting the cylindrical specimens transversely, perpendicular to their longitudinal axis, obtaining circular cross-sections slices. A portable hand-

polishing device, which uses diamond-impregnated rubber disks (No.50 [coarse], 100, 400, 800, 1500, 3000 [very fine]), was found most suitable Sanchez et al., (2016), as it does not use loose abrasive powders that can fill up cracks/voids in the concrete. Due to the consistency observed in preliminary data, where variation between samples of the same set (calculated as deviation/average value) remained consistently low (<10%), it was deemed sufficient to analyze only one polished section (100 cm² [15.5 in.²]) from 12 selected specimens out of the 24 samples.

4.3.3 DRI-Based Analysis

The Damage Rating Index (DRI) was conducted following the current protocol established by Sanchez et al. (2015). The assessment included the identification and counting of various distress features, with particular attention to cracks in the cement paste with and without reaction products (i.e., CCP and CCP-RP). The DRI values were computed based on the weighting factors presented in Table 4-1 and the results were normalized to 100 cm^2.

In addition to the conventional Damage Rating Index (DRI) method, the extended DRI version, proposed by (Sanchez et al., 2015, 2016; Sanchez et al., 2017), was incorporated to enhance the assessment of corrosion-induced damage. In this approach, microscopic distress features (Table 4-1) were evaluated in absolute (counts) and relative (%) terms without applying weighting factors. This method provided a broader perspective on crack patterns and damage progression in corrosion-affected concrete.

In the extended DRI, we report crack density as the normalized summation of cracks per unit area (counts/100 cm²) and normalized crack area as the total projected crack area relative to the analyzed surface. A key feature of the extended DRI is the calculation of the cracking area, representing the total sum of open cracks in the cement paste with and without reaction products. To further validate the reliability of the DRI in assessing corrosion-induced damage, ImageJ software was employed for precise quantification. Cracks were manually traced, their projected areas measured, and the total crack area computed to determine the extent of deterioration. To enable a comparative analysis across different C/D and W/C ratios, the total crack area (cm²) was normalized by dividing it by the total analyzed surface area (cm²) of the specimen (Equation 4-1). The normalized values were then expressed per 100 cm², ensuring consistency in evaluating the

severity of corrosion-induced cracking among the tested samples (Equation 4-1). Thus, crack density emphasizes how frequently cracks occur (counts/100 cm²), whereas normalized crack area captures how much surface is affected (area/100 cm²).

$$\text{Normalized Crack Area} = \left(\frac{\sum Total\ Crack\ Area\ (cm2)}{Surface\ Area\ (cm2)}\right) \times 100 \qquad \text{(Equation 4-1)}$$

Additionally, spatial crack distribution analysis was performed to examine how cracks propagate under different W/C and C/D ratios. A qualitative damage rating system was also introduced, assigning damage levels from 0 (no damage) to 5 (severe damage) to complement the quantitative DRI results.

4.4 Results

4.4.1 Quantitative Assessment of Damage Using DRI

Figure 4-3 illustrates the DRI charts obtained from the corrosion-affected concrete samples, showcasing the overall distribution of the distinct microscopic damage features such as cracks in the cement paste (CCP), and cracks with reaction products in the cement paste (CCP-RP).

In general, the DRI values of the samples increase with increasing W/C ratio and decreasing C/D ratio, indicating a higher extent of corrosion-induced deterioration. Reduced concrete cover, corresponding to lower C/D ratios, accelerates damage by offering less physical resistance to crack propagation, thereby exacerbating deterioration. At the same time, higher W/C ratios lead to higher overall porosity, which in turn reduces the quality of concrete microstructure and thus mechanical properties of the material, further increasing its vulnerability to cracking. This interaction between material composition and geometric detailing underscores the complex mechanisms governing corrosion-induced deterioration in reinforced concrete.

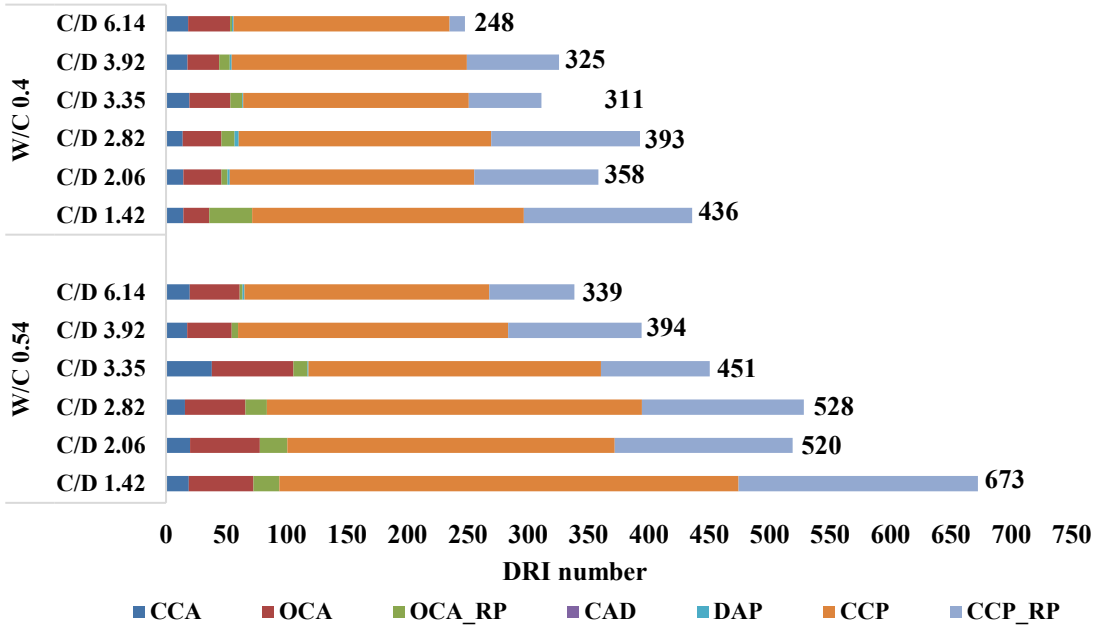

Figure 4-3 - DRI assessment for the different concrete specimens in the study

Figure 4-3 demonstrates that for samples with the same C/D ratio, the W/C ratio significantly influences the severity of damage. For example, at a C/D ratio of 1.42, the DRI value for the sample with a W/C ratio of 0.54 is 673, compared to 436 for the sample with a W/C ratio of 0.4. This substantial difference emphasizes the detrimental effect of the concrete microstructure on the overall damage. A similar trend is observed for the other C/D ratios. At C/D 2.06, the DRI value rises from 358 for W/C 0.4 to 520 for W/C 0.54. Likewise, for C/D 2.82, the DRI value increases from 393 for W/C 0.4 to 528 for W/C 0.54. Conversely, for the samples with the highest C/D ratio of 6.14, the effect of the W/C ratio is less pronounced. The DRI values for these samples are 339 for W/C = 0.54 and 248 for W/C = 0.4. Likewise, for C/D 3.92, the DRI value increases less from 325 for W/C 0.4 to 394 for W/C 0.54.

When examining samples with the same W/C ratio but different C/D ratio, further trends emerge. At a W/C ratio of 0.54, the sample with a C/D ratio of 1.42 exhibits a DRI of 673 which is more, pronounced than the value of 520 observed for the sample with a C/D ratio of 2.06; similarly, at a W/C ratio of 0.4, the DRI decreases from 436 for a C/D ratio of 1.42 to 393 for a C/D ratio of 2.82. The results clearly demonstrate the sensitivity and reliability of the DRI protocol in capturing the

degrees of damage induced by corrosion, highlighting its potential as a diagnostic tool for microscopic deterioration.

Finally, it is important to note that, as expected, damage features such as closed cracks in aggregate (CCA), open cracks in aggregate (OCA), and open cracks with reaction products in aggregate (OCA-RP), do not seem to be relevant to corrosion-induced deterioration, as only a few damage features of this kind were observed. Therefore, to focus on the microscopic features related to corrosion-induced development, only features directly linked to this mechanism (i.e., CCP and CCP-RP) will be assessed and discussed in the subsequent sections of this study. Moreover, the extended version of the DRI (i.e., absolute counts and percentages of CCP and CCP-RP without applying the weighting factors) will be used to further understand and explain the impact of W/C and C/D ratios on corrosion-induced damage.

4.4.2 Impact of W/C and C/D on Corrosion-Induced Deterioration

Figure 4-4 presents the normalized crack densities of CCP and CCP-RP as a function of C/D ratios, for both W/C mixtures and geometries, independent of sample size.

Interestingly, for W/C 0.4, the total normalized crack densities decrease progressively with increasing C/D ratio, ranging from 77 cracks per 100 cm² at C/D of 1.42 to 47 at C/D of 6.14. Within this range, CCP values remain relatively stable between 37 and 48, while CCP-RP shows a clear downward trend from 29 to just 3.

Likewise, the W/C 0.54 specimens also exhibit a decrease trend of crack density as a function of C/D, ranging from 122 at C/D 1.42 to 51 at C/D 6.14. The CCP values range from 37 to 80, and CCP-RP decrease from 42 to 13 with increasing C/D. The elevated counts in this group reflect the greater porosity and lower mechanical resistance of high-W/C concrete, which facilitates the generation and propagation of cracks. Finally, although crack density decreases with increasing C/D, the reduction is more gradual in W/C 0.44 than in W/C 0.54.

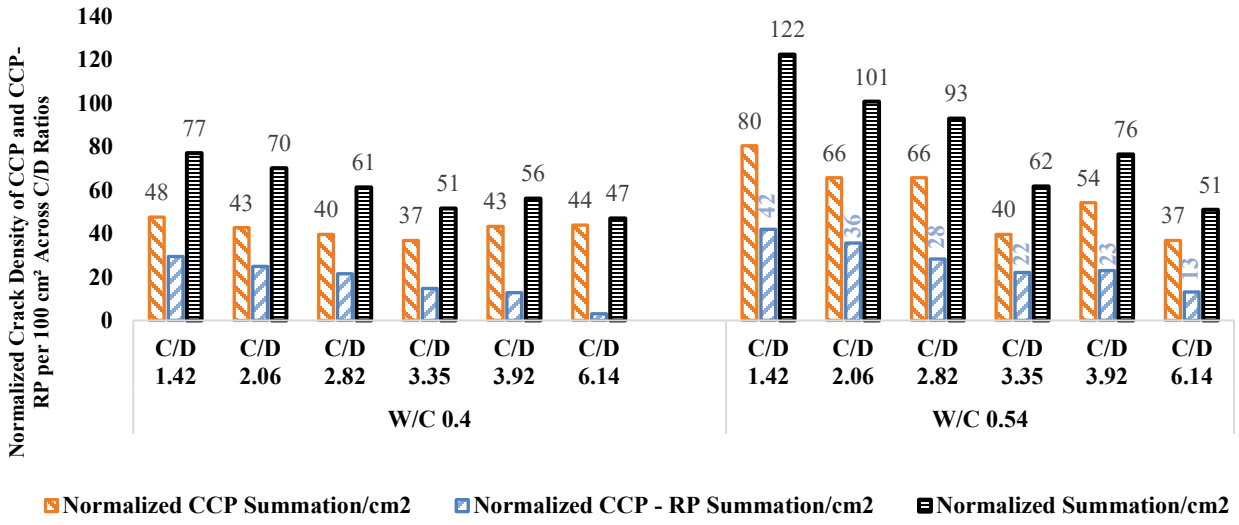

Figure 4-4 - Normalized crack densities of CCP and CCP-RP as a function of C/D ratios

4.5 Discussion

4.5.1 Sensitivity of the DRI to Evaluating Corrosion-Induced Damage

The extended version of the DRI includes both absolute counts and percentage-based representations of distress features without the application of weighting factors. While absolute counts provide a basic quantitative overview, percentage-based analysis provides a more generalized evaluation of the damage process caused by corrosion particularly on the importance of CCP and CCP-RP on the overall damage.

Figure 4-5 presents the comparative percentages of CCP and CCP-RP across varying water-to-cement (W/C) and concrete cover-to-rebar diameter (C/D) ratios. In specimens with W/C = 0.4, a clear trend is observed: the contribution of CCP towards the total observed damage increases with rising C/D, from around 60% at C/D = 1.42 to over 90% at C/D = 6.14. This indicates that thicker concrete covers significantly hinder the outward migration of corrosion products, resulting in microcracking that predominantly manifests as clean CCP-type fractures. Concurrently, the proportion of CCP-RP features drops steeply—falling below 10% at high C/D ratios—demonstrating that the thicker concrete matrix restricts the movement and accumulation of corrosion by-products within the crack network, even at equivalent corrosion levels.

In contrast, at W/C = 0.54, the percentage of CCP remains relatively steady across all C/D values, increasing only slightly from 66% to 73%. Meanwhile, CCP-RP remains consistently present, fluctuating around 27% to 34%. This important contribution of CCP-RP suggests that the higher porosity and permeability of the 0.54 mixture facilitate the migration of corrosion products, even when the cover thickness increases.

The results highlight that the microstructural development of cracking features is jointly influenced by both W/C and C/D ratios. In low W/C mixtures, the dominance of CCP at high C/D reflects reduced permeability and denser microstructure, which limit the transport of ionic species and confine corrosion activity closer to the steel surface. This reduces the likelihood of extensive reaction product formation within the crack network. Conversely, in high W/C mixtures, the concrete's increased porosity promotes greater ingress of moisture and oxygen, facilitating both the initiation of microcracking and the spread of corrosion products, leading to a more balanced distribution of CCP and CCP-RP features—even at higher C/D ratios.

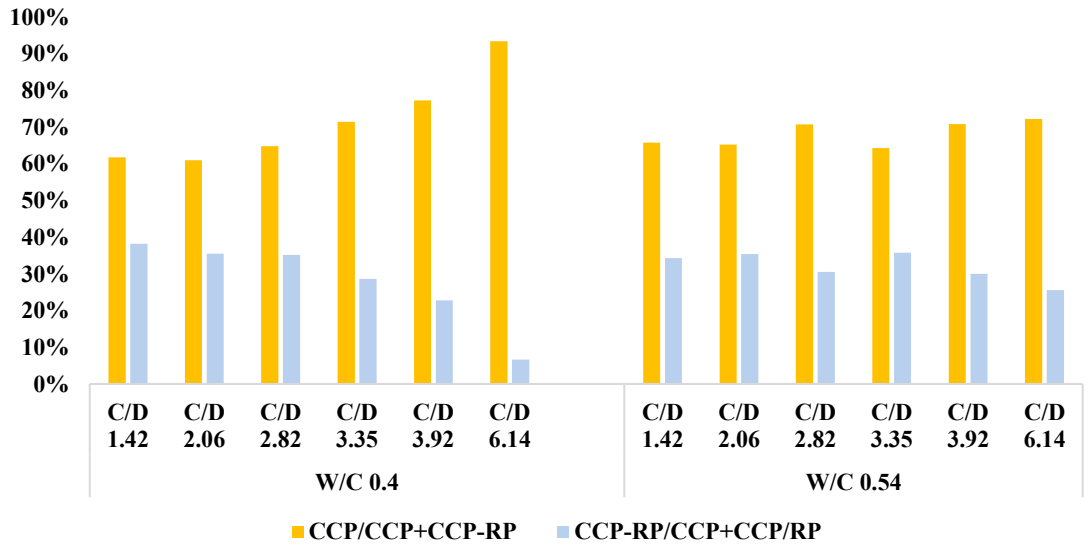

Figure 4-5 - Percentage distribution of CCP and CCP-RP relative to total distress features (CCP + CCP-RP) for each mixture and C/D ratio

4.5.2 Damage Classification Framework

The evaluation of corrosion-induced cracking in the RC using the extended DRI provides a systematic framework for mapping the progression of damage across varying W/C and C/D ratios.

While models for crack initiation and propagation under corrosion have been extensively explored in prior research (Alonso et al., 1998, Andrade 2017), this study uniquely validates the DRI as a sensitive and reliable tool for quantifying corrosion-induced deterioration. The extended DRI quantifies key damage features, specifically cracks in the cement paste (CCP) and cracks with reaction products in the cement paste (CCP-RP), enabling a detailed numerical representation of damage severity. To enhance this evaluation, visual inspections shown in Figure 4-6 serve as a complementary approach, highlighting the patterns, orientation, and extent of damage while corroborating the quantitative results obtained from crack area measurements and summation indices. This dual assessment approach bridges the gap between numerical data and physical observations, ensuring a holistic evaluation of corrosion-induced distress in concrete.

The visual assessments in Figure 4-6 reveals distinct crack patterns and propagation mechanisms, influenced by both W/C and C/D ratios. The observed cracks predominantly propagate longitudinally along the reinforcement, indicating a stress-relief mechanism due to corrosion expansion. The severity of cracking decreases with increasing C/D ratio, as observed in both normalized crack areas and summation indices, which aligns with the higher tensile capacity of thicker concrete covers that delay corrosion-induced damage. For W/C 0.54 specimens, cracks appear earlier and propagate more extensively than W/C 0.4 samples, reflecting the weaker microstructure of high W/C concrete. These findings confirm that crack development follows a progressive mechanism, where micro-cracks initiate around the reinforcement, extend radially, and eventually coalesce into larger longitudinal and interconnected cracks. The strong correlation between observed crack propagation, normalized crack area measurements, and extended DRI summation values demonstrates that the extended DRI method successfully captures corrosion-induced cracking with high sensitivity.

To define the damage levels in this study, the DRI ranges were adapted from a multi-level assessment framework for ASR-affected concrete, as proposed by (Sanchez et al., 2017, 2020). While the deterioration mechanisms of ASR and corrosion differ, the classification system provides a structured approach to categorizing varying degrees of corrosion damage in reinforced concrete. The classification is based on measured DRI values, complemented by normalized crack area measurements and visual inspections. Table 4-6 outlines the degrees of corrosion-induced damage severity for this study. The five damage levels are defined in the following:

- Level 0: No observable damage.

This level corresponds to specimens with no detectable damage. In this study, none of the specimens were classified under this category, as all exhibited measurable deterioration.

- Level 1: Minimal damage with very minor cracking.

Specimens with DRI values ranging from 100 to 200 fall under this category, indicating minor visual cracking. For instance, specimens with a C/D ratio of 6.14 at W/C 0.4 with DRI value of 192 exhibited very limited cracking, underscoring the protective influence of a thicker concrete cover.

- Level 2: Minor damage with slight cracking and limited progression.

This level includes specimens with DRI values ranging from 201 to 330, indicating limited crack progression. Examples include C/D ratios of 3.35 and 3.92 at W/C 0.4 and C/D 6.14 at W/C 0.54, with normalized crack areas ranging from 1 to 2%.

- Level 3: Moderate damage with noticeable cracking and early signs of reaction products.

Specimens with DRI values ranging from 331 to 500 fall under this category, indicating significant cracking accompanied by the presence of reaction products. Notable examples include specimens with C/D of 3.35 at W/C = 0.54 (DRI = 332), C/D of 2.82 at W/C = 0.4 (DRI = 332), and C/D of 3.92 at W/C = 0.54 (DRI = 334). Additionally, samples with C/D of 1.42 at W/C = 0.4 (DRI = 364) and C/D of 2.06 at W/C = 0.54 (DRI = 418) fall within this range and show pronounced deterioration. The specimen with C/D of 2.06 at W/C = 0.4, which had a slightly lower DRI value of 305, also exhibited a normalized crack area of 2%, reflecting a clear progression in damage severity.

- Level 4: Severe damage with extensive cracking and visible reaction products.

This level corresponds to DRI values ranging from 501 to 600, reflecting extensive cracking and significant deterioration. Additionally, specimens with the higher W/C ratio of 0.54, such as C/D of 1.42 (DRI = 579), displayed normalized crack areas ranging from 3% to 5%, underscoring the significant deterioration caused by corrosion.

- Level 5: Extreme damage with extensive cracking and substantial deterioration.

For specimens with DRI values exceeding 600, this level represents extensive damage with a fully interconnected cracking network, which may importantly impact the structural performance of critical infrastructure. Although no specimens in this study reached this level, it serves as a theoretical benchmark for extreme damage severity.

This classification system reinforces the capacity of DRI to translate numerical data into a meaningful depiction of damage severity, thereby validating its potential as a diagnostic tool for corrosion-induced deterioration. The incorporation of visual inspection further substantiates the DRI results by providing a tangible representation of the deterioration trends. For example, the alignment between normalized summation counts, normalized crack area measurements, and visual observations demonstrates the sensitivity of DRI in capturing variations in damage severity attributable to changes in W/C and C/D ratios

Table 4-6 - DRI assessment results of corrosion-affected concrete

W/C	Type	Classification of Corrosion Levels	DRI	CCP	CCP-RP	$\frac{CCP}{DRI}$	$\frac{CCP-RP}{DRI}$	$\frac{CCP}{CCP-RP}$	Normalized Summation/ cm^2*	Normalized CCP Summation/cm^2	Normalized CCP - RP Summation/cm^2	Normalized $\frac{CCP}{CCP-RP}$	Area of Cracks cm^2	**Normalized Area of Cracks %
0.4	1.42	Severe	364	225	139	0.62	0.38	1.62	62	48	29.4	1.62	1.268	3
	2.06	Minor	305	203	103	0.66	0.34	1.97	66	43	21.8	1.95	1.890	2
	2.82	Moderate	332	209	123	0.63	0.37	1.70	63	40	23.5	1.68	0.815	2
	3.35	Minor	247	187	60	0.76	0.24	3.12	76	37	11.9	3.10	2.102	1
	3.92	Minor	271	195	76	0.72	0.28	2.55	72	43	16.9	2.57	0.987	1
	6.14	Minimal	192	179	13	0.93	0.07	14.09	93	44	3.1	14.09	1.121	1
0.54	1.42	Severe	579	380	198	0.66	0.34	1.92	66	80	41.9	1.92	2.295	5
	2.06	Moderate	418	271	147	0.65	0.35	1.84	65	66	35.7	1.84	3.231	4
	2.82	Moderate	445	311	134	0.70	0.30	2.32	70	66	28.3	2.32	1.558	4
	3.35	Moderate	332	242	90	0.73	0.27	2.69	73	40	14.8	2.68	3.223	2
	3.92	Moderate	334	224	111	0.67	0.33	2.02	67	52	25.0	2.08	1.602	2
	6.14	Minor	273	203	70	0.74	0.26	2.88	74	37	13.0	2.85	1.921	1

Note: * Crack density = normalized summation (counts/100 cm^2); ** Normalized crack area = projected crack area/100 cm^2.

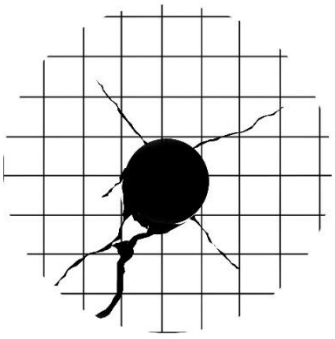

a) W/C 0.4, C/D 1.42

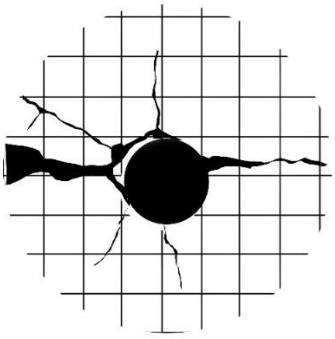

b) W/C 0.54, C/D 1.42

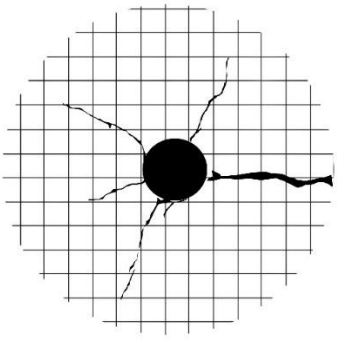

c) W/C 0.4, C/D 2.06

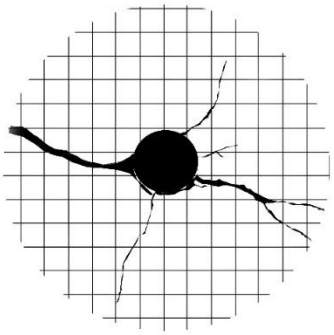

d) W/C 0.54, C/D 2.06

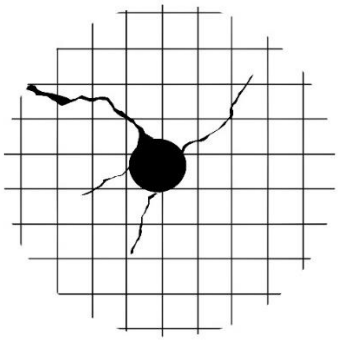

e) W/C 0.4, C/D 2.82

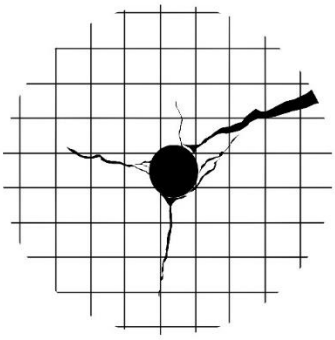

f) W/C 0.54, C/D 2.82

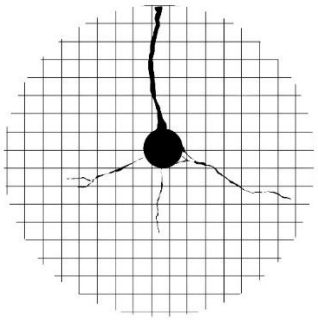

g) W/C 0.4, C/D 3.35

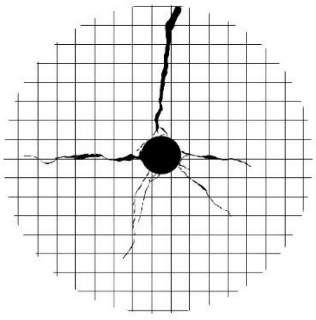

h) W/C 0.54, C/D 3.35

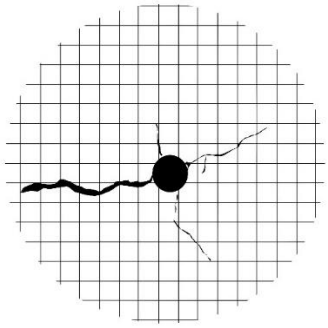

i) W/C 0.4, C/D 3.35

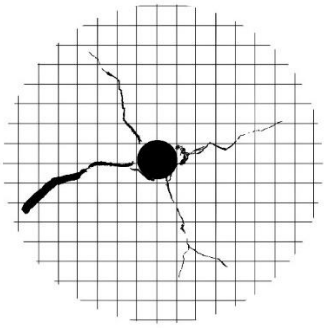

j) W/C 0.54, C/D 3.35

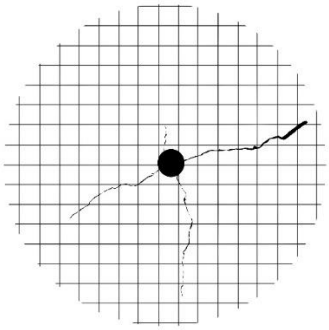

k) W/C 0.4, C/D 6.14

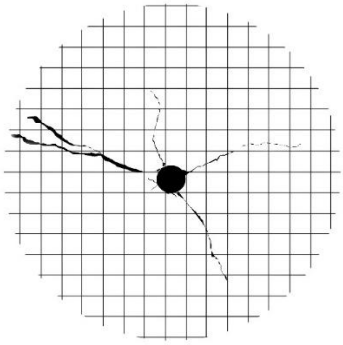

l) W/C 0.54, C/D 6.14

Figure 4-6- Visual Inspection of Crack Propagation

4.6. Conclusions

This study investigated the applicability and sensitivity of the DRI for quantifying corrosion-induced damage in reinforced concrete of varying W/C and C/D ratios. Through the integration of conventional and extended DRI methodologies, alongside normalized crack analysis and visual inspections, the research provides robust evidence that DRI is an effective and reliable tool for capturing the extent and severity of corrosion-related microstructural damage. The following key findings were drawn from the experimental results:

- DRI successfully captured corrosion-induced deterioration in all specimens, revealing a strong correlation between DRI values and governing material and detailing parameters such as W/C and C/D ratios.
- Higher W/C ratios consistently resulted in elevated DRI values, increased crack densities, and greater presence of CCP-RP, reflecting enhanced porosity and more aggressive corrosion progression.
- Lower C/D ratios intensified damage, as thinner concrete covers provided reduced tensile capacity, promoting faster crack propagation and higher DRI scores.
- CCP (cracks in the cement paste) became increasingly dominant in low W/C and high C/D mixtures, indicating that dense concrete microstructures confined corrosion activity near the reinforcement and limited the movement of reaction products.
- CCP-RP (cracks with reaction products in the cement paste) were significantly more prominent in high W/C mixtures, even at larger C/D ratios, due to higher permeability and sustained transport of corrosion by-products.
- The extended DRI method, incorporating absolute counts, percentages, and normalized crack areas, provided a detailed understanding of crack evolution and allowed for more refined classification of corrosion severity.
- A damage classification system was adapted to define five levels of corrosion-induced deterioration. These levels were validated through agreement among DRI values, normalized crack areas, and visual crack mapping.

- Visual inspections aligned with quantitative indicators, revealing longitudinal and radial crack patterns that intensified with increasing permeability and reduced concrete cover, further supporting DRI's diagnostic value.

Overall, the study establishes that both the conventional and extended versions of the DRI offer a comprehensive and sensitive approach for diagnosing corrosion-induced damage in reinforced concrete. This dual methodology enables better-informed decisions in maintenance planning, structural evaluation, and service-life forecasting.

4.7. References

ACI Committee 318. (2019). *ACI CODE-318-19(22): Building code requirements for structural concrete and commentary (Reapproved 2022)*. Farmington Hills, MI: American Concrete Institute.

Ahmad, S. (2003). *Reinforcement corrosion in concrete structures, its monitoring and service life prediction – A review*. Cement and Concrete Composites, 25(4–5), 459–471. Elsevier. https://doi.org/10.1016/S0958-9465(02)00086-0.

Allan, M. L. (1995). *Probability of corrosion-induced cracking in reinforced concrete*. Cement and Concrete Research, 25(6), 1171–1190. https://doi.org/10.1016/0008-8846(95)00091-D

Cheng, W., Fan, Z., & Tan, K. H. (2023). *Characterisation of corrosion-induced crack in concrete using ultrasonic diffuse coda wave*. Ultrasonics, 128, 106883. Elsevier. https://doi.org/10.1016/j.ultras.2022.106883

CSA Group. (2019). *CSA A23.1:19 / CSA A23.2:19 – Concrete materials and methods of concrete construction / Test methods and standard practices for concrete*. Toronto, ON: Canadian Standards Association.

Guzmán, S., & Gálvez, J. C. (2017). *Modelling of concrete cover cracking due to non-uniform corrosion of reinforcing steel*. Construction and Building Materials, 155, 1063–1071. Elsevier. https://doi.org/10.1016/j.conbuildmat.2017.08.082

Hong, S., Wiggenhauser, H., Helmerich, R., Dong, B., Dong, P., & Xing, F. (2017). *Long-term monitoring of reinforcement corrosion in concrete using ground penetrating radar*. Corrosion Science, 114, 123–132. Elsevier. https://doi.org/10.1016/j.corsci.2016.11.003

Hwang, W., & Ann, K. Y. (2023). *Determination of rust formation to cracking at the steel–concrete interface by corrosion of steel in concrete*. Construction and Building Materials, 367, 130215. Elsevier. https://doi.org/10.1016/j.conbuildmat.2022.130215

Li, Q., Jin, X., Yan, D., Fu, C., & Xu, J. (2021). *Study of wiring method on accelerated corrosion of steel bars in concrete*. Construction and Building Materials, 269, 121286. Elsevier. https://doi.org/10.1016/j.conbuildmat.2020.121286

Liu, Y., & Weyers, R. E. (1998). *Modeling the time-to-corrosion cracking in chloride contaminated reinforced concrete structures*. ACI Materials Journal, 95(6), 675–680. American Concrete Institute.

Lu, C., Jin, W., & Liu, R. (2011). *Reinforcement corrosion-induced cover cracking and its time prediction for reinforced concrete structures*. Corrosion Science, 53(4), 1337–1347. https://doi.org/10.1016/j.corsci.2010.12.026

Mak, M. W. T., Desnerck, P., & Lees, J. M. (2019). *Corrosion-induced cracking and bond strength in reinforced concrete*. Construction and Building Materials, 208, 228–241. Elsevier. https://doi.org/10.1016/j.conbuildmat.2019.02.151

Marcotte, T. D., & Hansson, C. M. (2007). *Corrosion products that form on steel within cement paste*. Materials and Structures / Matériaux et Constructions, 40(3), 325–340. https://doi.org/10.1617/s11527-006-9170-4

Rodrigues, R., Gaboreau, S., Gance, J., Ignatiadis, I., & Betelu, S. (2021). *Reinforced concrete structures: A review of corrosion mechanisms and advances in electrical methods for corrosion monitoring*. Construction and Building Materials, 269, 121240. Elsevier. https://doi.org/10.1016/j.conbuildmat.2020.121240

Sanchez, L. F. M., Fournier, B., Jolin, M., Bedoya, M. A. B., Bastien, J., & Duchesne, J. (2016). *Use of Damage Rating Index to quantify alkali-silica reaction damage in concrete: Fine versus coarse aggregate*. ACI Materials Journal, 113(4), 395–407. American Concrete Institute. https://doi.org/10.14359/51688983

Sanchez, L. F. M., Fournier, B., Jolin, M., & Duchesne, J. (2015). *Reliable quantification of AAR damage through assessment of the Damage Rating Index (DRI)*. Cement and Concrete Research, 67, 74–92. Elsevier. https://doi.org/10.1016/j.cemconres.2014.08.002

Tian, Y., Zhang, G., Ye, H., Zeng, Q., Zhang, Z., Tian, Z., Jin, X., Jin, N., Chen, Z., & Wang, J. (2023). *Corrosion of steel rebar in concrete induced by chloride ions under natural environments*. Construction and Building Materials, 369, 130504. Elsevier. https://doi.org/10.1016/j.conbuildmat.2023.130504

Van Steen, C., Van Beirendonck, T., Vrijdaghs, R., Hendriks, M. A. N., & Verstrynge, E. (2023). *A two-phased modelling approach for corrosion-induced concrete cracking and bond deterioration in reinforced concrete*. Engineering Structures, 294, 116624. Elsevier. https://doi.org/10.1016/j.engstruct.2023.116624

Vidal, T., Castel, A., & François, R. (2004). *Analyzing crack width to predict corrosion in reinforced concrete*. Cement and Concrete Research, 34(1), 165–174. Pergamon. https://doi.org/10.1016/S0008-8846(03)00246-1

Wang, Y. Z., Zhao, Y. X., Gong, F. Y., Dong, J. F., & Maekawa, K. (2022). *Developing a three-dimensional finite element analysis approach to simulate corrosion-induced concrete cracking in reinforced concrete beams*. Engineering Structures, 257, 114072. Elsevier. https://doi.org/10.1016/j.engstruct.2022.114072

Zhang, Y., & Su, R. K. L. (2020). *Experimental investigation of the process of corrosion-caused cover cracking*. Construction and Building Materials, 253, 119166. Elsevier. https://doi.org/10.1016/j.conbuildmat.2020.119166

Zhao, Y., Dong, J., Wu, Y., & Jin, W. (2016). *Corrosion-induced concrete cracking model considering corrosion product-filled paste at the concrete/steel interface*. Construction and Building Materials, 116, 273–280. Elsevier. https://doi.org/10.1016/j.conbuildmat.2016.04.097

Zhao, Y., & Jin, W. (2016). *Damage analysis and cracking model of reinforced concrete structures with rebar corrosion*. In Steel corrosion-induced concrete cracking (pp. 55–77). Butterworth-Heinemann. https://doi.org/10.1016/B978-0-12-809197-5.00004-9

Zhou, Y., Gencturk, B., Willam, K., & Attar, A. (2015). *Carbonation-induced and chloride-induced corrosion in reinforced concrete structures*. Journal of Materials in Civil Engineering, 27(9), 0401209. American Society of Civil Engineers (ASCE). https://doi.org/10.1061/(ASCE)MT.1943-5533.0001209

5 Concluding Remarks

5.1. Conclusions

This study evaluated the applicability and sensitivity of the Damage Rating Index (DRI) as a microscopic tool for quantifying corrosion-induced damage in reinforced concrete (RC) structures with varying water-to-cement (W/C) and concrete cover-to-rebar diameter (C/D) ratios. Based on an extensive experimental campaign combining conventional DRI analysis, extended quantitative assessments (normalized crack areas and crack densities), and visual inspections, the following conclusions were drawn:

- **DRI Sensitivity**: The DRI successfully captured microstructural distress features in concrete associated with corrosion-induced cracking. The results confirmed that DRI values strongly correlate with key material and detailing parameters, notably W/C and C/D ratios. This establishes the DRI as a reliable semi-quantitative tool not only for internal swelling reactions, for which it was initially developed, but also for corrosion-induced damage.
- **Extended DRI Analysis**: Incorporating normalized crack densities and crack areas provided a more comprehensive understanding of crack development, strengthening the correlation between microscopic features and deterioration severity. Using both crack density (frequency) and normalized crack area (extent) distinguished many small cracks from fewer, wider/longer cracks, refining the interpretation of corrosion damage.
- **Dominance of Specific Microscopic Features**:
  Cracks in cement paste (CCP) became increasingly dominant in low W/C and high C/D mixtures, suggesting limited transport of corrosion products due to denser microstructures. In contrast, CCP-RP features were more prevalent in high W/C mixtures across all C/D levels, demonstrating the permeability-driven movement of corrosion by-products.
- **Visual-DRI Correlation**: Integration of DRI data with visual inspections confirmed that micro-level damage features strongly correlate with macro-level cracking patterns and support the proposed classification of damage severity.

- **Damage Classification Framework**: A five-level corrosion damage model was developed, enabling structured interpretation of deterioration based on DRI values and normalized crack characteristics.
- **Practical Implications**: The study demonstrates that DRI, originally developed for ASR and ISR, can be reliably extended to assess corrosion-induced cracking. Its ability to characterize damage in a semi-quantitative and reproducible manner makes it a valuable addition to current diagnostic practices for evaluating the structural condition of RC elements. It should be noted, however, that the accelerated corrosion regime employed in this study likely promoted a more uniform corrosion process. Since the morphology of the corroded reinforcing bars was not evaluated, localized or pitting effects cannot be inferred from the presented results.

This work establishes a new research pathway by applying the Damage Rating Index (DRI) — originally developed for internal swelling reactions — to corrosion-induced deterioration in reinforced concrete. Through extended DRI analysis (normalized crack densities and areas), the study demonstrates the method's sensitivity to corrosion-driven microstructural changes and its reproducibility across different W/C and C/D ratios. Importantly, the proposed five-level corrosion-induced damage classification framework provides a structured, semi-quantitative tool that bridges microscopic damage assessment with macroscopic visual observations. This constitutes a novel contribution to durability diagnostics in RC structures.

5.2. Recommendations for Future Work

While the present study demonstrated the DRI's effectiveness in a controlled laboratory setting, additional work is recommended to strengthen its application scope:

- **Expanded Corrosion Levels:**
  Investigating specimens subjected to higher degrees of corrosion (e.g., 10%, 15% steel mass loss) would provide a broader understanding of DRI sensitivity across progressive stages of deterioration. This would help determine whether the proposed classification framework remains robust at advanced levels of reinforcement corrosion.

- **Integration with Existing Damage Framework:**

  Future research could explore linking the corrosion damage classification developed in this study with frameworks for other deterioration mechanisms, such as alkali–silica reaction (ASR), delayed ettringite formation (DEF), and freeze–thaw (FT) damage. Such integration would enhance the applicability of DRI as a unified diagnostic tool for reinforced concrete deterioration.

- **Multi-Assessment: DRI with Non-Destructive Techniques:**

  Coupling DRI assessments with non-destructive testing methods (e.g., ground-penetrating radar, acoustic emission, or ultrasonic pulse velocity) could provide a comprehensive, multi-scale evaluation of deterioration. This combined approach would improve early detection capabilities and extend the practical utility of the DRI.

- **Field Validation:**

  Applying the DRI protocol to field-extracted cores from real, aged structures would validate laboratory findings under diverse exposure conditions, variable corrosion rates, and more complex deterioration patterns. Such validation is essential for confirming the reliability of the method in practice.

- **Enhanced Crack Characterization:**

  The current study focused on normalized crack areas and densities; however, future frameworks could also incorporate crack widths and lengths to provide a more complete quantification of damage severity and to strengthen the link between microscopic and macroscopic deterioration.

- **Automation of Crack Quantification**

  Integrating digital image analysis and machine learning tools for automatic quantification of petrographic damage features could reduce subjectivity, improve reproducibility, and enhance efficiency in applying the DRI protocol. Building on density and area, future work should include **crack width and length** to directly capture the opening and propagation, tightening links between serviceability and durability.